Journal of South American Earth Sciences 80 (2017) 272–290

Contents lists available at ScienceDirect

Journal of South American Earth Sciences

journal homepage: www.elsevier.com/locate/jsames

Tourmaline orbicules in peraluminous monzogranites of Argentina: A study case of fluid-rock interaction between leucogranite and country-rock metasediments

Raúl Lira [a, *], María F. Poklepovic [b]

[a] Consejo Nacional de Investigaciones Científicas y Técnicas – Museo de Mineralogía y Geología "Dr. A. Stelzner", FCEFyN-Universidad Nacional de Córdoba, V. Sarsfield 249, X5000JJC, Córdoba, Argentina
[b] Dirección Provincial de Vialidad, Los Pozos 2850, Córdoba, Argentina

ARTICLE INFO

Article history:
Received 9 February 2017
Accepted 24 September 2017
Available online 27 September 2017

Keywords:
Tourmaline orbicules
Leucogranite
Boron
Fluid-rock interaction
Country-rock metasediments
Argentina

ABSTRACT

Tourmaline orbicules hosted in peraluminous granites are documented worldwide. Seven occurrences were identified in Argentina. Petrography, mineral chemistry, whole-rock geochemistry mass balance and microthermometric studies were performed in orbicules formed at the cupola of a peraluminous A-type leucogranite (Los Riojanos pluton), as well as complementary investigation was achieved in other orbicules of similar geological setting. Mass balance computations in zoned orbicules consistently confirmed immobility of Si both in core and halo, immobility of K and little loss of Al during halo reactions. Elements gained and lost in the schorl-rich core are Fe, Al, Mg, Ti, Ba, Sr, Y and Zr, and Na, K, Rb and Nb, respectively; in the halo, K, Ba, Sr, Y, Zr and locally CaO, were gained, and Fe, Mg, Na, Al, Rb and Nb were lost. The schorl-rich core is enriched in LREE relative to the leucogranite host. A temperature-salinity plot from fluid inclusion data delineates a magmatic-meteoric mixing trend of diluting salinity with descending temperature. Computed δD_{H2O} values from Los Riojanos orbicule schorl suggest magmatic and magmatic-meteoric mixed origins. In Los Riojanos, mass balance constraints suggest that Fe, Mg, Ba, Sr and metallic traces like Zn and V (±Pb) were most likely derived from country-rock schists and gneisses through fluid-rock exchange reactions. A late magmatic-, volatile-rich- fluid exsolution scenario for the formation of orbicules is envisaged. Schorl crystallization was likely delayed to the latest stages of leucogranite consolidation, not only favored by the high diffusivity of B_2O_3 preferentially partitioned into the exsolved aqueous-rich fluid, but also likely limited to the low availability of Fe and Mg from the scarce granitic biotite, and to the high F^- content of the melt. The spatial confination of orbicules to the contact zone granite-metasediments suggests that orbicules were not formed until exsolved fluids reached the boundary with the biotite-rich country-rock.

1. Introduction

Minerals of the tourmaline supergroup occur in a large variety of lithologies, frequently as an accessory phase or, more rarely, as an important constituent in other specific rock types, such as tourmalinites. Its wide range of stability in terms of temperature, pressure, fluid and protolith composition, and the close relationship between mineral chemistry and rock type makes tourmaline an almost ubiquitous supergroup of minerals that can deliver valuable information about the petrogenesis of their host rocks (i.e., Henry and Guidotti, 1985; Hinsberg et al., 2011).

Members rich in Fe and Li (schorl-elbaite series) are common accessory minerals in felsic peraluminous granitoids and highly fractionated melts such as pegmatites and aplites; the variability of tourmaline chemical composition in haplogranitic systems has strongly contributed to the understanding of fractionation processes and evolutionary trends in felsic melts (Neiva, 1974; Buriánek and Novák, 2003; Buriánek and Žáček, 2015).

In metamorphic terrains, tourmaline minerals form as recrystallized products over detritic grains in protolithic sedimentary rocks leading to the origin of tourmaline–rich rocks composed of members of the dravite-schorl series, such as tourmalinites, which

* Corresponding author.
E-mail addresses: raul.lira@unc.edu.ar (R. Lira), fpoklepovic@gmail.com (M.F. Poklepovic).

https://doi.org/10.1016/j.jsames.2017.09.030
0895-9811/

are intimately related to the origin of base metal (Pb-Ag-Zn) stratabound deposits of the volcanic massive sulfide (VMS) type (Slack, 1982; Fieremans and De Paepe, 1982; Slack et al., 1984; Pesquera and Velasco, 1997). Tourmaline breccia pipes, normally spatially associated to magmatic-hydrothermal Cu-Mo porphyry systems are, as well, rich in members of the dravite-schorl series (Sillitoe and Sawkins, 1971; Sillitoe, 1985; Eichenlaub, 2007; Demirel et al., 2009; Dill et al., 2012). It is well known that tourmaline composition might be useful as a pathfinder in ore deposit exploration, being Mg-rich tourmaline normally associated to VMS (Pb-Zn-Ag) deposits, whereas schorl is indicator of Sn and W deposits (Slack, 1982; Taylor and Slack, 1984; Plimer, 1987; Slack et al., 1993; Hellingwerf et al., 1994; Slack, 1996; Jiang et al., 1998). Tourmaline minerals are also present in metasomatic and hydrothermal mineral assemblages associated to granite intrusions (Akçay et al., 1995; Slack, 1996).

Experimental data from granitic systems indicate that tourmaline stability depends on the availability of boron, temperature, pressure, the amount and fugacity of water, and the content of Al, Fe and Mg within the system (London et al., 1996; London, 1997, 1999, 2008). Crystallization of tourmaline occurs either as a magmatic process, well expressed in the LCT pegmatites (London, 2008) or as a subsolidus replacement mechanism developed during the post-magmatic stage, triggered by boron-rich fluids.

Tourmalinization of country rock is found to be a relatively widespread phenomenon as alteration aureoles enveloping boron-rich highly evolved felsic granites (London et al., 1996); a similar process under the form of nodules or orbicules hosted in highly evolved felsic granitic rocks is not as common, but remarkably similar in all worldwide occurrences. Their presentation, also referred to as nodules, clots, spots, nests, pockets or knots, is known since long time ago in different localities throughout the world (see Didier, 1973; Rozendaal and Bruwer, 1995; Balen and Broska, 2011; Boudreaux, 2014); their particular texture and contrasting colors in central Elba (Capo Bianco aplite sill, Perugini and Poli, 2007) seem to have even called the attention in ancient times of the mythic Jason and the Argonauts (Dini et al., 2007). The origin of concentrically zoned orbicules composed of schorl-rich cores and quartz-rich leucocratic halos was recently summarized by Balen and Broska (2011), who identified at least four main hypothesis that range from magmatic crystallization of boron-rich melts, post-magmatic (metasomatic-hydrothermal) replacement of previously crystallized granite (or pelitic xenoliths) by boron-rich fluids, to magmatic-hydrothermal processes related to the separation of an immiscible aqueous-, boron-rich melt from a granitic-, silicate-rich melt (e.g., Sinclair and Richardson, 1992; Samson and Sinclair, 1992; Shewfelt, 2005; Trumbull et al., 2008; Dini, 2011; Balen and Petrinec, 2011; Drivenes et al., 2015), plus their own interpretation that favors a late-stage boron-rich volatile fluid phase exsolved from crystallizing granite melt (devolatilization). Most hypotheses have in common that B-rich fluids would derive from felsic magmatic sources during late evolutionary stages of melt solidification (e.g., Buriánek and Novák, 2003, 2004; Jiang et al., 2003; and previous citations).

Lira (1985) described the geological setting, mineralogy and textural relationships of schorl-nodules from Los Riojanos pluton, a muscovite (±biotite) leucogranite located in the Achala batholith of the Eastern Pampean Ranges of Central Argentina. Tejerina (1985) found similar nodules in an aplitic granite of the El Carnero pluton (nowadays named El Hornito, Ortiz Suárez et al., 1997) in the northern edge of Sierra de San Luis, also part of the Eastern Pampean Ranges. In Catamarca province were identified by Colombo (2007) in Rodeo Gerván, Papachacra, Belén Department; in this locality, tourmaline orbicules are deformed, lense-shaped, hosted in porphyritic-, locally aplitic-granophyric monzogranite dykes of pre-Devonian age. New findings in the country were reported in Ordovician granites from Jujuy province (Elortegui Palacios, 2011, and previous references therein); orbicules are hosted in the Las Burras alkali-feldspar miarolitic leucogranite and less frequently in the enclosing Churcal monzogranite. One of the authors (RL) made new findings in Salta province, in a small (<1 km^2) Ordovician peraluminous garnet-, ±tourmaline-bearing leucogranite, east of Salar Centenario between Quebrada Burruyacu and Quebrada del Puesto, in the Serranía de Ochaqui, southern Puna (Viramonte et al., 2007), and NW of Andalgalá city, Catamarca province, in the felsic aplitic-granitic facies of the Capillitas batholith (e.g., Rossi et al., 2002). Deformed, oval-shaped tourmaline orbicules similar to those from Papachacra dykes were reported by F. Parra and F. Cecenarro (personal communication) in Ordovician orthogneisses from the Quebrada Cajón del Mojón, Sierra de Velasco, ~15 km east of Pinchas, La Rioja province; in the same area other undeformed orbicules occur in post-ordovician aplitic intrusives (Figs. 1 and 2).

This contribution is intended to approach a better understanding of element mobility in a boron-rich environment. Tourmaline orbicules from two of the seven occurrences listed for Argentina were selected for study (i.e., Los Riojanos and El Hornito), preferentially over the first occurrence. The tourmaline orbicule genesis is interpreted based on field constraints, petrographic analyses, mineral chemistry, whole rock geochemistry, microthermometric and some δD data, as a final product derived from a fluid/rock interaction process between leucogranite exsolved fluids and medium-to high-grade metasedimentary country rocks.

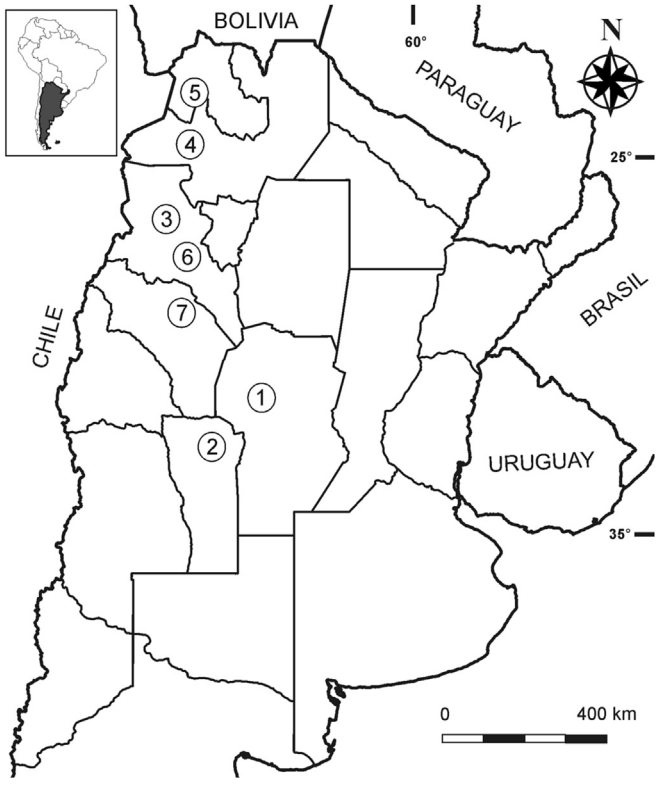

Fig. 1. Location of schorl orbicules findings in Argentina. 1- Los Riojanos, Achala batholith, 2- El Hornito, Sierra de San Luis, 3- Rodeo Gerván, Papachacra, 4- Serranía de Ochaqui, Puna, 5- Las Burras and Churcal granites, Puna, 6- NW of Andalgalá, Capillitas Batholith, 7- East of Pinchas, Sierra de Velasco.

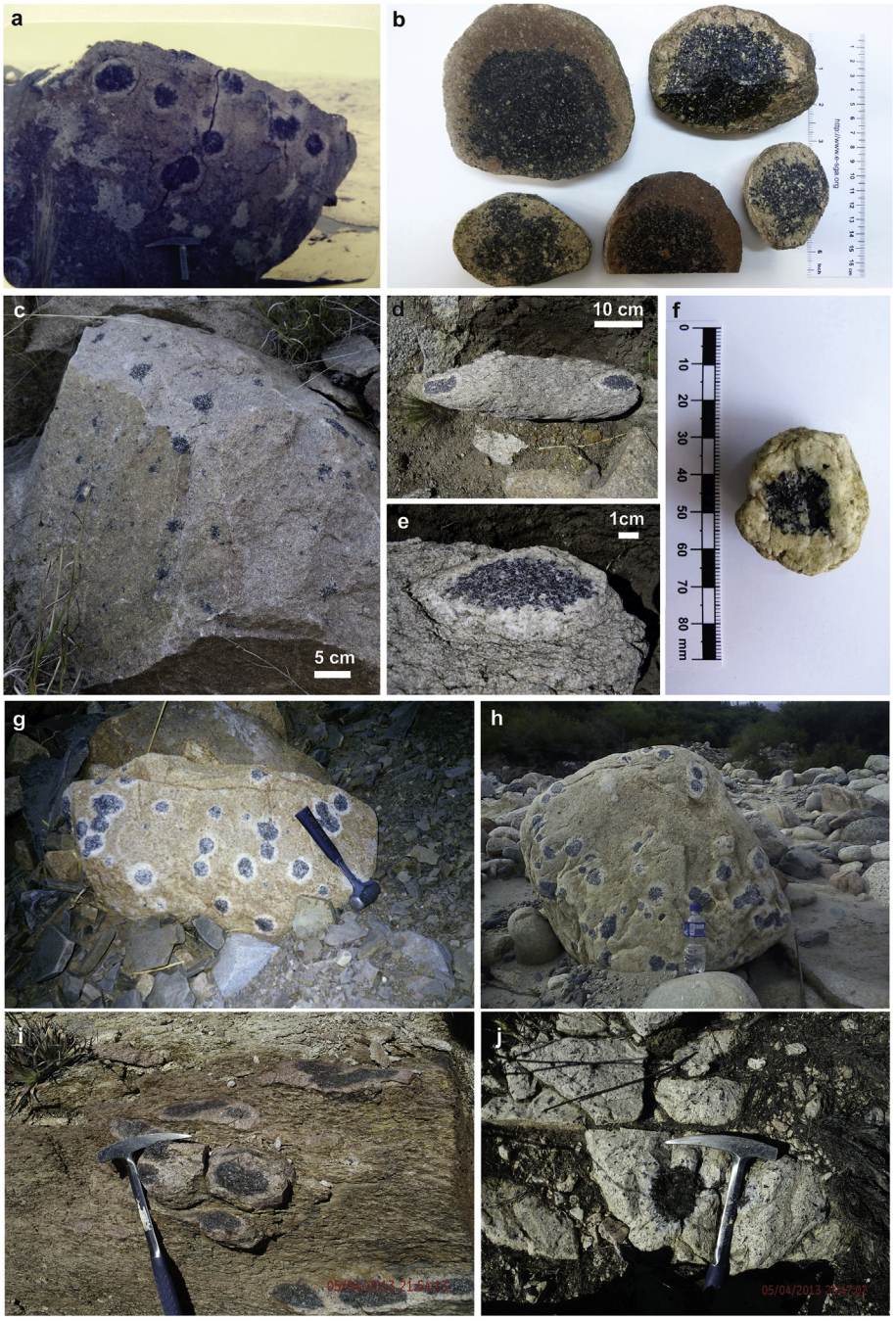

Fig. 2. Schorl orbicules from the Pampean Ranges and Puna regions of central and northwestern Argentina. Los Riojanos (**a-b**), El Hornito (**c**), Rodeo Gerván (**d-e**), Serranía de Ochaqui (**f**), Las Burras (**g**), NW of Andalgalá (**h**), and East of Pinchas (**i-j**).

2. Materials and methods

Major and some trace element whole rock analyses of original samples were done in X-RAL SGS laboratories in Canada by X-Ray fluorescence on 2 g-powdered fused discs; in 4 samples (as indicated in Table 1) some trace elements (Co, Ni, Cu, Zn, Mo, Ag, Cd, Pb, Hg, Sb, As, Au) were analyzed by X-Ray fluorescence on pressed pellets; other elements were performed in the laboratories of Actlabs (Canada), by ICP and ICP-MS on 5 g-pulverized samples fused with Li-metaborate/tetraborate, dissolved in weak HNO_3. X-Ray fluorescence analyses have the following detection limits: major elements, TiO_2, MnO and P_2O_5 = 0.01%; lower detection limits for selected trace elements are shown in brackets in ppm: Rb, Sr, Y, Zr and Nb (2), and Ba (20); Co, Ni, Cu, Zn, Mo, Ag, Cd, Pb, Hg, Sb, As and Au (variable between 2 and 3). Detection limits for ICP- and ICP-MS analyses are 0.01% for major elements and 0.001% for TiO_2 and MnO; detection limits for trace elements are shown in brackets in ppm: Zn (30), Ni and Cr (20), As, Pb, V and Zr (5), Ba (3), Mo, Sr and Rb (2), Be, Co, Ga, Ge, Sc, Sn, W and Y (1), Ag, Sb and Sc (0.5), Bi (0.4), Hf, In and Nb (0.2), Ta, Tl, U and Th (0.1). Detection limits for REE ICP-MS analyses from ACTLABS are: La, Ce, Nd, Sm, Gd, Tb, Dy, Ho, Er and Yb (0.1), Pr, Eu and Tm (0.05), and Yb (0.04).

Tourmaline-supergroup minerals were analyzed in a CAMECA SX 50 electron probe microanalyzer with software of the SX100

Table 1
Whole-rock major and trace element analyses.

Wt.%	Los Riojanos											El Hornito
	LR2 gneiss	LR4 gneiss	LR6 gneiss	LRO leucogr	LR4 leucogr	7011 leucogr	Orbicule A*		Orbicule B*		Orbicule C	Orbicule D
							halo	core	halo	core	core	core
SiO_2	67.24	72.51	71.08	74.63	75.06	75.11	75.40	70.70	75.20	70.90	70.85	71.20
TiO_2	0.89	0.87	0.70	0.09	0.05	0.09	0.14	0.19	0.17	0.24	0.19	0.17
Al_2O_3	14.09	11.77	12.24	14.46	13.72	14.02	13.60	16.40	13.60	17.10	15.70	15.85
Fe_2O_3	5.87	4.96	5.00	0.98	0.81	1.00	0.65	4.49	0.98	4.61	4.16	3.68
MnO	0.07	0.09	0.08	0.04	0.04	0.04	0,01	0.05	0.00	0.05	0.09	0.06
MgO	2.33	1.95	2.33	0.14	0.08	0.13	0.10	1.13	0.10	1.16	0.95	0.91
CaO	1.49	1.51	1.48	0.37	0.45	0.37	0.59	0.37	0.38	0.31	0.62	0.45
Na_2O	2.60	2.61	2.11	3.47	3.88	3.38	3.11	2.36	2.91	2.35	1.76	2.34
K_2O	3.29	2.26	3.09	4.54	4.01	4.55	4.83	1.24	4.45	1.43	2.95	2.57
P_2O_5	0.20	0.18	0.13	0.28	0.38	0.30	0.40	0.22	0.26	0.16	0.26	0.24
LOI	1.43	1.58	1.43	1.11	1.35	1.09	1.20	1.35	1.35	1.80	1.80	1.34
F	–	–	–	–	0.12	0.18	–	–	–	–	–	–
Total	99.50	100.29	99.66	100.11	99.95	100.26	100.03	98.50	99.40	100.11	99.33	98.81
B_2O_3	–	–	–	–	0.0039	0.0013	–	3.46	–	3.44	3.44	3.80
ppm												
Sc	15	13	13	–	2	4	–	–	–	–	–	–
Be	2	8	1	–	15	30	–	–	–	–	–	–
Ba	448	403	669	54	55	53	242	81	274	116	97	104
Rb	203	314	150	603	438	552	337	91	283	95	338	192
Sr	138	117	136	16	15	17	47	30	55	32	39	31
Y	33	37	37	11	6	10	44	26	40	26	23	28
Zr	298	309	207	43	27	45	124	107	124	104	86	102
Nb	21	14	12	50	35	37	29	8	28	10	10	10
Th	15	11	10	5	2	5	–	–	–	–	14	15
U	5	3	4	4	3	4	–	–	–	–	4	4
Zn	100	90	70	33	30	40	–	–	–	–	170	166
Sn	4	4	5	15	8	16	–	–	–	–	8	9
Ta	2	2	1	12	12	11	–	–	–	–	3	3
W	193	588	561	7	380	10	–	–	–	–	<1	1
Tl	2	2	1	4	3	4	–	–	–	–	2	2
Pb	23	14	24	12	16	27	–	–	–	–	33	26
Bi	<0.4	<0.4	<0.4	2	20	5	–	–	–	–	48	25
V	121	96	82	<5	10	<5	–	–	–	–	56	33
Ga	22	16	16	26	24	24	–	–	–	–	35	33
Cs	52	62	19	52	21	54	–	–	–	–	40	13
Hf	7.9	8.4	5.6	1.8	1.2	1.8	–	–	–	–	4.0	4.2
Cr	60	50	40	–	<20	<20	–	–	–	–	–	–
Co	29	63	57	–	34	<1	–	–	–	–	–	–
Ni	40	30	20	–	<20	<20	–	–	–	–	–	–
Cu	10	<10	<10	–	20	<10	–	–	–	–	–	–
Ge	2	2	2	–	2	3	–	–	–	–	–	–
As	<5	<5	<5	–	<5	<5	–	–	–	–	–	–
Mo	<2	<2	<2	–	<2	<2	–	–	–	–	–	–
Ag	<0.5	<0.5	<0.5	–	<0.5	<0.5	–	–	–	–	–	–
In	<0.2	<0.2	<0.2	–	<0.2	<0.2	–	–	–	–	–	–
Sb	1.8	<0.5	<0.5	–	<0.5	0.6	–	–	–	–	–	–
δ (g/cm^3)	–	–	–	2.65	–	–	2.64	2.80	2.59	2.76	2.77	–

(*) X-Ray fluorescence analyses from X-Ral SGS laboratories; remaining correspond to ICP- and ICP-MS analyses from ACTLABS; e.g. < 2: below detection limit. Anomalous W values are due to contamination by milling in a tungsten carbide ring mill. δ = measured rock density.

model, in the Department of Geology of Brigham Young University (Provo, Utah); analytical conditions were the following: 15 Kv, 10 nA, electron beam diameter of 5 mμ; natural and synthetic standards used were: flúor-phlogopite and Durango apatite for F^-, jadeíte for Na, MgO for Mg, anorthite for Al, orthoclase for Si and K, Durango apatite for P, "scapolite" for Cl, wollastonite for Ca, titanite for Ti, spessartine garnet for Mn, and fayalite for Fe. Plagioclase and muscovite analyses were performed at the LAMARX, FaMAF, Universidad Nacional Córdoba), using a Jeol JXA 8230 electron probe microanalyzer; analytical conditions were: beam size = 10 μm diameter, current = 20 nA and 15 Kv. Natural and synthetic standards were used. In both cases, data were reduced after Pouchou and Pichoir (1985) correction factors.

Fluid inclusion petrography was done in double polished thin sections of quartz and tourmaline chips of ~100–150 μm thick; microthermometric measurements were made in a Fluid Inc. heating-freezing stage calibrated with Syn Flinc synthetic standards; instrumental precision was ±0.1 °C between −56.6 °C and +660.4 °C. Temperatures of homogenization and of freezing-point depression were processed with the FLINCOR 1.4 software (Brown, 1989). The δD_{schorl} values were acquired at the Department of Geological Sciences of Indiana University (Bloomington, Indiana, USA) applying the procedure of Sharp et al. (2001).

3. Host- and country-rock geology, mineralogy and geochemistry

3.1. Los Riojanos (LR) leucogranite

The LR leucomonzogranite outcrops in the central western margin of the large (ca. 2500 km^2) peraluminous A-type Devonian Achala batholith, at latitude 31° 26′ S and longitude 64° 48′ W, in

the Eastern Pampean Ranges of Central Argentina (e.g., Dorais et al., 1997; Rapela et al., 2008; Lira et al., 2012; Lira and Sfragulla, 2014, and references therein).

The intrusive body is one of the highest differentiated facies of the whole batholith (Lira, 1985; Lira and Kirschbaum, 1990; Lira and Sfragulla, 2014) and integrates the Achala series defined by Demange et al. (1993, 1994, 1996), mostly composed of porphyritic to coarse equigranular biotite-muscovite monzogranites, which account for ~ 70% of the total batholith exposure. The LR granite is a small sized, NNW-elongated, oval-shaped body of ~5.5 km^2 (Fig. 3), located in a peripheral position respect to the main batholithic body, in intrusive contact with enclosing biotite gneisses of Cambrian age. Along its contact with the metasedimentary country rocks, the leucogranite shows marked textural variations from miarolitic-pegmatite, in direct contact with gneisses, passing inward into an aplitic facies, and in smooth transition into the areally dominant medium grained, equigranular granitic texture.

The hololeucocratic LR granite is composed in average by 36 vol % quartz, 31% plagioclase ($An_{<13}$), 28% K-spar (highly ordered microcline), variable contents of muscovite within 5–9 vol % (primary and secondary), and, sporadically < 1% of relic biotite (Lira, 1985, 1987; Lira and Kirschbaum, 1990; Lira and Sfragulla, 2014). Accesory and alteration minerals are apatite, zircón, rutile, uraninite, albite, Fe-oxides/hydroxides, and clay minerals; tourmaline is absent within the leucogranite mass. Quartz occurs as anhedral grains with invariably undulouse extinction, frequently intergrown with microcline developing a micrographic texture. Plagioclase is subhedral, incipiently replaced by sericite. Tartan twinned microcline is typically perthitic, weakly altered to clay minerals. Muscovite occurs in subhedral crystals, most of it weakly brownish and pleochroic evidencing phengitic composition. Relic biotite after strong muscovitization is rare; its composition corresponds to annite (X_{Fe} within the range 0.81–0.88); muscovites are compositionally true muscovites and phengites with 6.42 apfu Si and molar Fe between 0.67 and 0.73 (Demange et al., 1996).

The aplitic border facies is mineralogically similar to the equigranular facies, with the particularity of carrying a higher content of biotite (though < 2% modal), most of it partially transformed into muscovite and stained by secondary Fe-oxides/hydroxides; fan-shaped aggregates of schorl are distinctive of the aplitic border zone.

ASI values between 1.3 and 1.5 evidence the peraluminous nature of the LR pluton, as indicated by high modal values of muscovite and normative corundum. Lira and Kirschbaum (1990) highlighted the main chemical features of this granite (in oxide weigth %) characterized by low Ca (0.40–0.60), Ti (0.12–0.15), Mg (<0.08), and Fe^{3+}_T (1.18–1.45), and elevated concentrations of Na (2.41–4.60) and K (4.14–5.08). Enrichments in Rb, Li and Y suggest a high degree of specialization of the melt.

Late to postmagmatic hydrothermal alteration includes widespread sericitization and muscovitization after plagioclase and biotite. Tourmalinization has strongly affected the Los Riojanos granite and enclosing country rock, where at least four distinct morphological and paragenetic tourmaline types were described (Lira, 1985); type I: orbicular tourmaline, type II: fan-shaped prismatic tourmaline aggregates found in the bordering pegmatitic unit, type III: crosscutting quartz-tourmaline veins, and type IV: flat aggregates of radial, fibrous tourmaline interlayered in country rock gneisses and schists.

Structurally controlled barren quartz-muscovite greisenization

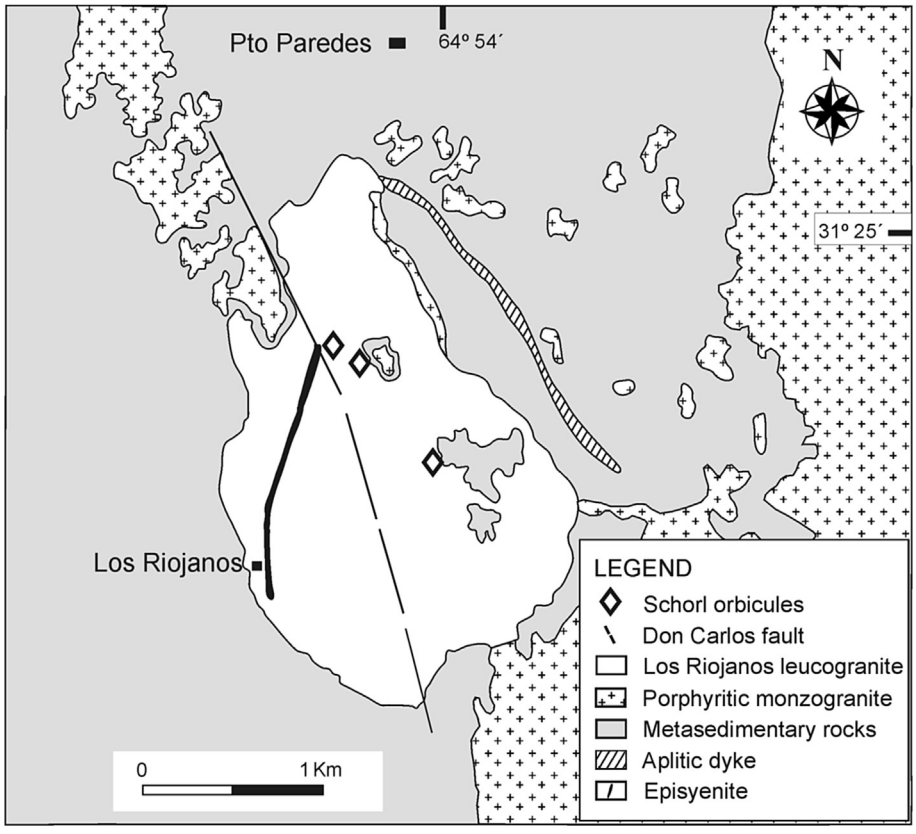

Fig. 3. Geological map of Los Riojanos leucogranite in the central-western slope of the Sierra Grande, Achala batholith, simplified from Lira (1985) and Poklepovic (2007).

and U-mineralized feldsphatic epysienites are also part of the postmagmatic cooling history of the LR pluton (Lira, 1987; Lira et al., 1996).

3.2. El Hornito (EH) pluton

The EH pluton is located in the southern part of the Sierras Pampeanas Orientales, northern of the San Luis ranges at 65° 42′ W and 32° 20′ S, positioned like a NE satellite of the Devonian Las Chacras-Piedras Coloradas batholith (Brogioni, 1993). Ortiz Suárez et al. (1997) described the geology of this pluton (Fig. 4). The size of the body is about 73 km^2, morphologically elongated in direction NE-SW; it has intruded quartz-mica schists and metaquartzites of Cambrian age, and produced hornfelses in its southern contact (Tejerina, 1985; Ortiz Suárez et al., 1997). Ortiz Suárez et al. (1997) interpreted the EH pluton as a shallow-seated postkynematic body intruded in an environment with marked thermal contrast. Three granitic facies were recognized, a NE located facies of medium to fine grained equigranular texture, a regionally dominant porphyritic facies with microcline megacrysts that intrudes the equigranular facies, and a tonalitic facies that crops out in its northern boundary. The EH pluton has been characterized by Ortiz Suárez et al. (1997) as calcalkaline, peraluminous of high-K_2O, enriched in HFS elements and depleted in Sr and Ba. Ortiz Suárez et al. (2009) redefined four main granite facies for the EH pluton (porphyritic, external, red granite and diorite enclaves and hybrid rocks); the porphyritic granite to granodiorite facies is the most widespread rock, it is cut by aplite and microgranite dykes, quartz veins and lamprophyres. This facies hosts abundant miarolitic cavities filled in by quartz, potassic feldspar and tourmaline.

Tourmaline orbicules are found spread in an aplitic body within the areally dominant porphyritic granite to granodiorite facies. Metamoprhic country rock xenoliths and roof pendants are present nearby; cross-cutting pegmatite and aplite dikes are also common in the area. The aplite body is composed of quartz, plagioclase, K-spar, biotite and scarce muscovite (Ortiz Suárez et al., 1997).

3.3. Tourmaline orbicules

3.3.1. Field occurrence

Tourmaline orbicules show remarkably similar fabrics, regardless of their worldwide distribution. The orbicules are built up of a dark core, largely composed of schorl, and a distinct quartz-enriched leucocratic rim; the sharp boundary between both zones is controlled by the disappearance of tourmaline. The outer boundary of the orbicules, i.e., the contact with the normal-, unaltered-granite host, develops at the outer boundary front of quartz growth, and constitutes a sharp concentric weakness surface where the orbicules physically liberate from the granite host after weathering processes. Being rounded or ellipsoidal and protected by a silica-rich shell, once released they accumulate by gravity in depressed zones.

Both in the LR and the EH plutons the field distribution pattern of tourmaline orbicules do not reveal any type of linear structural control, such as joint systems, fracture intersections or magmatic fluidality.

In the LR granite, orbicules are distributed throughout the equigranular facies, at the apical, roof zone of the pluton, close to the enclosing metasedimentary country rock; localized concentrations can be as high as 5 to 10 vol %. In this locality, orbicules are specifically concentrated east of Don Carlos NNW-SSE reverse fault (Fig. 3), in the uplifted block, where metamorphic roof pendants and xenoliths are still preserved from erosion. Metasedimentary rocks of the area are two-mica (biotite > muscovite) gneisses.

At the EH pluton, orbicules occur in an aplitic facies of the pluton, also in the vicinities of metamorphic roof pendants and

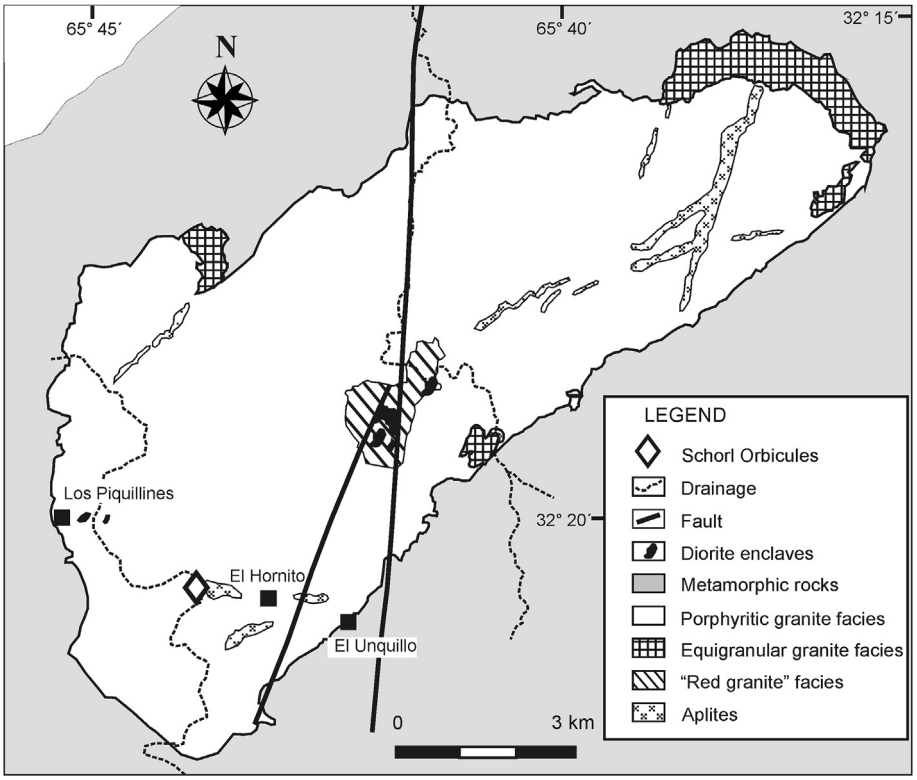

Fig. 4. Geological map of El Hornito pluton, northern boundary of Sierra de San Luis, modified from Ortiz Suárez et al. (1997, 2009).

xenoliths (Fig. 4).

In both localities orbicules are non-deformed, spherical to ovoidal, varying in diameter from 3 to 12 cm, rarely up to ~18 cm; at El Hornito they are significantly smaller, most being <5 cm. In Los Riojanos the leucocratic haloes range from 0.5 to 3 cm thick, normally keeping a core to halo thickness ratio of 3:1; in some orbicules tourmaline has developed a dendritic habit at the outer core-inner halo boundary (equivalent to the "starburst" morphology of Shewfelt, 2005). Except for the dominating spherical to ellipsoidal patterns and subordinated "starburst" textures, the large variety of morphologies well documented by Shewfelt (2005) in the Scrubber Granite of Western Australia were not observed in any of both described localities. Perugini and Poli (2007) have mathematically modeled growth conditions of orbicules in relationship with the variability of orbicule morphologies.

3.3.2. Petrography

In Los Riojanos, the felsic halo that rims the tourmaline-rich core of the orbicules is mineralogically and texturally similar to the host equigranular facies, except for the absence of relic biotite replaced by phengite. The muscovite developed in the leucocratic halo is anhedral, and strongly poiquilitic, suggesting a pervasive growth over paragenetic euhedral-subhedral quartz. Within the felsic halo both alkali-feldspars are altered to clay minerals. Alteration of plagioclase proceeded with incipient muscovitization; during this reaction the low molar fraction of An in plagioclase becomes patchy calcite. Within the schorl-rich core, muscovite is variably converted into schorl through cleavages showing reactive borders.

The earliest stage of tourmalinization starts with veinlet or patchy schorl that replaces microcline, indistinctly of the sodic or potassic fractions of microcline. Relics of larger K-feldspar grains are proofs of the pseudomorphic replacing process, which is accompanied by silica precipitation under the form of euhedral to subhedral quartz crystals, varying in size from 50 to 350 mμ, which is included by schorl growth; necessary silica for quartz co-precipitation with schorl could be derived from K-feldspar breakdown. Advanced, almost complete tranformation shows a mosaic of schorl intergrown with suhedral to euhedral quartz. Schorl is strongly pleochroic with Z = olive green and X = light brown; some crystal borders show irregular patchs of light bluish hues. Secondary quartz within the melanocratic core includes bundles of acicular rutile; few smaller prismatic crystals of schorl could be found included in quartz.

Relic granitic plagioclase found within the schorl orbicules halo range in composition from 13.4 (core) to 12.8 (rim) An mol %; some plagioclase relics within the schorl-rich core have albite rims ~ 2% An mol %. In the core, plagioclase breaks down into radial aggregates of muscovite and is replaced by sericite along cleavages and twinning planes. With increasing tourmalinization, remnant plagioclase not affected by muscovitization becomes replaced by schorl. A particular, acicular tourmaline type projects from replaced K-feldspar towards partially muscovitized plagioclase forming fibrous bunches of colourless to light blue tourmaline. Tourmaline that replaces K-feldspar shows weak chromatic zoning evolving from core toward rim. Iron is present in the system as seen in tourmaline microfractures and crystal borders which are frequently stained by Fe-oxides, as well as tiny hematite crystals disseminated in sericitized plagioclase.

3.3.3. Whole rock geochemistry

Whole rock compositions of leucogranite, country rock gneiss and tourmaline orbicules are listed in Tables 1 and 2. The geochemistry of the orbicules was studied separately by zone; concentric zones were carefully sliced using a diamond saw on the largest orbicules. The analyses were restricted to the LR orbicules, because the reduced size of the EH granite orbicules impeded a sufficiently clean zone separation.

The orbicules core is rich in boron varying between ~1000 and 1200 ppm, values which obviously are much larger than not only the average content of felsic and silica-rich rocks (10–30 ppm) but also higher than extreme enrichments (i.e., 500 ppm London et al., 1996); the elemental B content in LR leucogranite ranges from 4 to 12 ppm whereas in the orbicule's core is concentrated up to ~ 1200 ppm, that is an increase of ~100–300 times. The boron content reflects a direct relationship with the increase on Fe and Mg in the core indicating that schorl rules the distribution of these elements: for example, values as low as 1 wt % Fe_2O_3 and 0.15 wt % MgO in the host leucogranite raises up to 17 wt % Fe_2O_3 and 1.2 wt % MgO in the orbicules core. The correlation of K_2O against B_2O_3 is negative, confirming replacing textures that show K-spar breakdown and schorl formation.

Fig. 5 depicts variation of a few major elements across alteration zoning from protholithic granite to core through felsic halo; in the halo-core boundary the sharp decline in K coincides with abrupt increase of Mg (similar to Fe), reflecting microcline consumption to form schorl. The progressive Na decrease from host leucogranite toward core responds to plagioclase replacement either by muscovitization in the felsic halo or by tourmalinization in the core; muscovitization in the felsic halo consumed plagioclase to form muscovite probably with available K_2O from K-feldspar breakdown in the core after schorl formation, fact that is also supported by a noticeable increase in K_2O. Equivalent data from Seagull, Canada

Table 2
Whole-rock REE analyses.

ppm	LR2 gneiss	LR5 gneiss	LR6 gneiss	LRO leucogr	LR4 leucogr	7011 leucogr	Orb C core	Orb D core
La	48.7	41.4	31.0	11.7	3.0	6.4	17.6	22.3
Ce	95.5	77.7	60.9	19.7	6.1	13.2	41.9	40.6
Pr	11.2	9.8	7.4	2.3	0.8	1.6	4.0	5.8
Nd	42.9	38.8	28.3	8.4	3.3	6.1	14.9	21.8
Sm	8.3	7.5	5.8	1.8	0.8	1.4	3.6	5.2
Eu	1.4	1.4	1.2	0.1	0.1	0.1	0.4	0.4
Gd	6.9	6.6	5.1	1.6	0.7	1.2	3.4	4.9
Tb	1.2	1.2	1.0	0.3	0.2	0.3	0.7	0.9
Dy	6.5	6.9	6.3	1.9	1.2	1.9	4.0	5.0
Ho	1.2	1.4	1.3	0.3	0.2	0.4	0.8	0.9
Er	3.0	4.1	3.9	1.2	0.7	1.1	2.2	2.6
Tm	0.4	0.6	0.6	0.2	0.1	0.2	0.3	0.4
Yb	2.5	3.8	3.5	1.3	0.8	1.3	2.0	2.3
Lu	0.4	0.6	0.5	0.2	0.1	0.2	0.3	0.3
Total	230.1	201.8	156.8	51.1	18.1	35.4	96.2	113.3

Detection limits (in ppm) for ICP-MS analyses are: La, Ce, Nd, Sm, Gd, Tb, Dy, Ho, Er and Yb (0.1), Pr, Eu and Tm (0.05), and Yb (0.04).

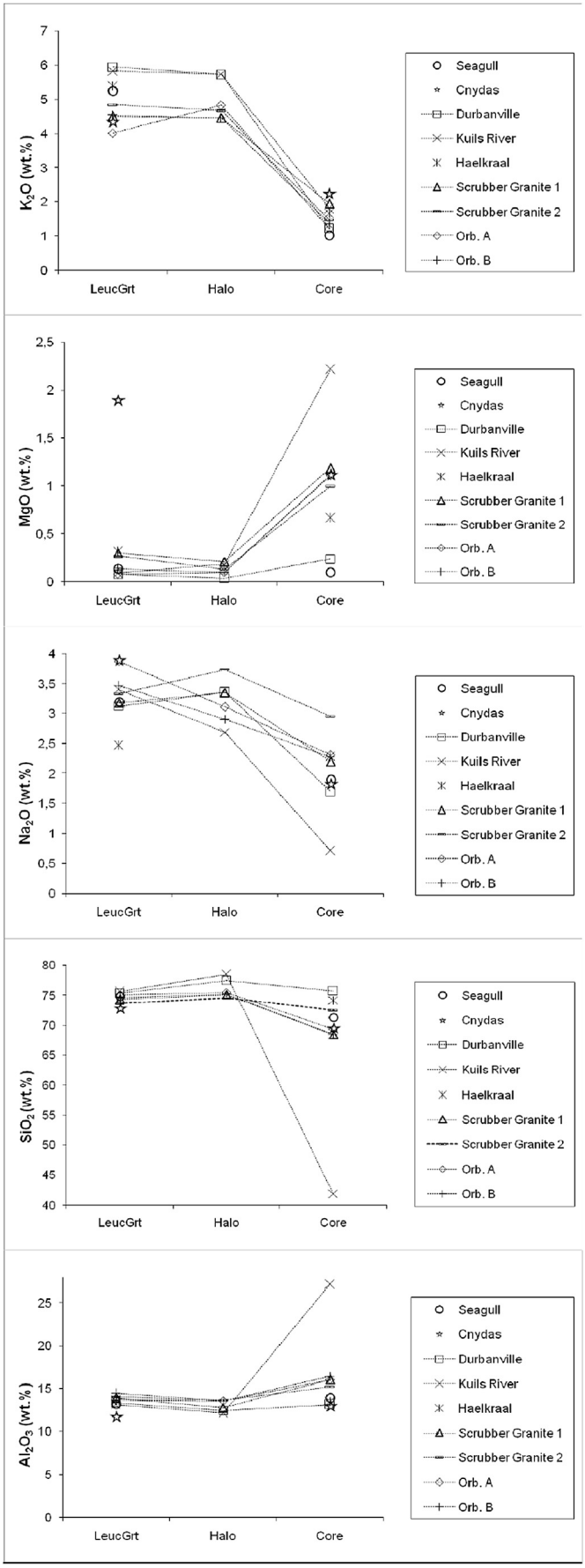

(Sinclair and Richardson, 1992), Cnydas, Durbanville, Kuils River, and Haelkraal, South Africa (Rozendaal and Bruwer, 1995), and from the Scrubber Granite, Western Australia (Shewfelt, 2005), are added in Fig. 5, and all except one (Mg from Cnydas) show similar behavior. Silica increases about 1 wt % in the felsic halo and decreases significantly in the core (~4 wt %) respect to the protholitic host. The alumina content slightly decreases in the halo and increases in the core. The Ca content is practically preserved, as shown texturally by the remnants of An-richer plagioclase cores and also by patchy calcite found in the leucocratic halo. TiO_2 increases gradually from host granite toward the dark core, most likely in correspondence with the formation of bunches of acicular rutile included in neoformed quartz intergrown with tourmaline.

Regarding trace element distribution, the strongly differentiated host leucogranite has been characterized by high Rb and low Ba and Sr contents. The Rb/Ba ratio decreases from the host granite (range = 26 to 8, includying values of Montenegro, 2002) toward the orbicule (range = 3.5 to 0.8, considering both halo and core); both elements could be released from microcline breakdown, with Ba being retained by muscovite that forms after plagioclase. The weak enrichment of Sr within the core could be the result of plagioclase breakdown with Sr preservation in the neoformed tourmaline (King et al., 1988), and/or enrichment by concentration of remnants af An-rich cores of plagioclase. Nevertheless, Ba and Sr are concentrated in country rock schist and gneisses up to ~8–10 times more than in leucogranite (see Table 1), therefore addition from this external source is not unlikely. The schorl-rich cores are enriched in Ba, Sr, Zr, V, Zn, Pb, Ga, Hf, Bi and Th, and depleted in Rb relative to the host leucogranite (Table 1). High contents of Zn and anomalous Pb values in the melanocratic cores (166–170 ppm and 26–33 ppm, respectively) are probably contained in schorl (e.g., King et al., 1988; Henry and Dutrow, 2001). Oppositely, the Sn and W contents in the orbicules core are similar or lower than in the host granite (see Table 1).

The LR leucogranite has very low REE totals (18–51 ppm, Table 2), with a pronounced Eu/Eu* anomaly when normalized to Boynton's (1984) chondrite (0.25–0.45), which provides further evidence of the high degree of fractionation of the leucogranite melt. Normalized values of Gd-Tb-Dy-Ho and Er-Tm-Yb-Lu show a convex M-type "tetrad" effect (Masuda et al., 1987; Irber, 1999; Poklepovic and Lira, 2005; Poklepovic, 2007) which suggest fluid-rock interaction; this effect is normally found in highly evolved granites where a volatile-rich phase (principally F) coexists with an alkali-rich silicate melt (Irber, 1999; Zhenhua et al., 2002; Monecke et al., 2002; Takahashi et al., 2002).

In orbicule C, tourmalinization of the core produced a noticeable increase of total REE (≅ 88%, 51.1–96.2 ppm), from 43.8 to 82.1 ppm for LREE and from 7.1 to 13.7 ppm for the HREE. Shewfelt (2005) identified concentrations of LREE preferentially into the schorl-rich core over the halo of the tourmaline nodules of the Paleoproterozoic Scrubber Granite of Western Australia; secondary fluorcarbonates bastnäsite and synchysite were found associated with quartz and hematite filling fractures between tourmaline, quartz and relic feldspars in the core, and between quartz and feldspars in the halo and in the host granite; though Shewfelt (2005) made no comments about the potential origin of these carbonates, they probably formed after hydrothermal alteration of LREE-enriched schorl. Neiva (1974) noticed that granitic schorl is enriched in Ce,

Fig. 5. Representative mobile major element compositional variation from host leucogranite (sample LR0) through the halo to the schorl-rich core of orbicules from Los Riojanos, compared to orbicules from other well studied world localities: Seagull batholith, Yukon Territories (Sinclair and Richardson, 1992), Cnydas, Durbanville, Kuils River and Haelkraal, Cape Granite Suite, South Africa (Rozendaal and Bruwer, 1995), and from the Scrubber Granite, Western Australia (Shewfelt, 2005).

Nd, Sm, Gd, Tb, Dy and Er relative to associated aplites and pegmatites.

Values normalized to Boynton (1984) chondrite (Fig. 6) show a similar design for both the protholitic granite (samples LR-0, LR-4, 7011) and the orbicules core (orbicules C and D). The Eu anomaly does not vary significantly (Eu/Eu* = 0.25 to 0.38) and the La_N/Sm_N (4.08–3.05) and Lu_N/Gd_N (0.96–0.71) show a higher concentration of light and intermediate REEs. The orbicule core maintains a convex, M-type profile (Akagi et al., 1994), though the negative Ho anomaly decreases noticeably (Ho/Ho* = 0.82 to 0.97), so does the positive anomaly of Tb (Tb/Tb* = 1.14 to 1.07). The quantification of the 3rd and 4th lanthanide groups (T_3 = Gd-Tb-Dy-Ho, T_4 = Er-Tm-Yb-Lu; Irber, 1999), including the leucogranite and the core of the orbicules, show a less pronounced convexity due to decreasing values of T_3 (from 1.8 to 0.07) and T_4 (from 0.05 to 0.01). Data computed from Montenegro (2002) shows that the T_3 tetrad effect in the LR unaltered leucogranite is even more pronounced, yielding values between 0.21 and 0.53; these values could be indicative of fluid-rock interaction between the leucogranite and a tourmalinizing fluid with a concave REE pattern of the W-type, which causes the reduction of the T_3 and T_4 tetrad effect, being noticeable the decreased negative Ho and positive Tb anomalies with progressive fluid-rock interaction.

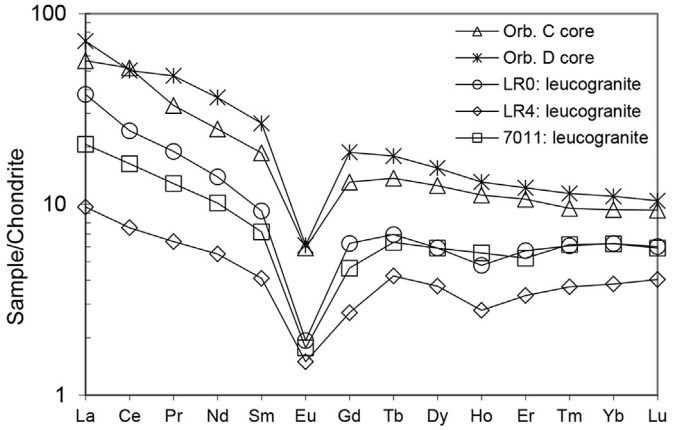

Fig. 6. REE spider diagram normalized to Boynton (1984) chondrite. LR0, LR4 and 7011: Los Riojanos leucogranite), Orb. C and Orb. D: schorl-rich cores of Los Riojanos and El Hornito orbicules, respectively.

Table 3
Schorl electron probe microanalyses.

	Los Riojanos					El Hornito			
	1a	1b	1c	2a	2b	1a	1b	2a	2b
SiO_2	35.31	35.59	35.46	35.23	35.47	35.02	34.54	34.64	34.30
TiO_2	0.52	0.49	0.58	0.68	0.64	0.30	0.59	0.44	0.55
Al_2O_3	33.40	34.19	33.91	34.19	34.15	34.89	33.30	33.97	33.02
FeO	10.64	11.01	10.46	11.08	11.09	10.76	11.69	11.22	11.64
MnO	0.10	0.15	0.11	0.20	0.00	0.33	0.44	0.27	0.26
MgO	3.44	3.50	3.53	3.00	3.16	3.63	3.71	3.83	4.03
CaO	0.14	0.13	0.14	0.16	0.15	0.21	0.28	0.30	0.35
Na_2O	2.14	2.02	2.12	2.16	2.09	1.95	2.16	2.10	2.10
K_2O	0.18	0.10	0.08	0.27	0.06	0.05	0.05	0.05	0.07
F	0.54	0.39	0.55	0.51	0.41	0.30	0.48	0.51	0.48
Cl	0.06	0.01	0.01	0.14	0.02	0.00	0.01	0.00	0.01
Total	86.48	87.55	86.94	87.62	87.24	87.44	87.25	87.33	86.82
O=F,Cl	0.03	0.02	0.03	0.03	0.02	0.02	0.03	0.03	0.03
Total	86.45	87.53	86.91	87.59	87.22	87.42	87.22	87.30	86.79
Structural formula on the basis of 29 (O,OH,F,Cl)									
B	3.000	3.000	3.000	3.000	3.000	3.000	3.000	3.000	3.000
Si	5.888	5.850	5.866	5.822	5.852	5.758	5.759	5.746	5.748
Al_T	0.112	0.150	0.134	0.178	0.148	0.242	0.241	0.254	0.252
Al_Z	6.000	6.000	6.000	6.000	6.000	6.000	6.000	6.000	6.000
Al_Y	0.453	0.473	0.477	0.480	0.492	0.519	0.302	0.386	0.268
Ti	0.066	0.061	0.072	0.084	0.080	0.038	0.074	0.055	0.069
Fe^{2+}	1.483	1.513	1.447	1.532	1.530	1.479	1.629	1.556	1.630
Mn	0.015	0.020	0.016	0.028	0.000	0.045	0.062	0.038	0.037
Mg	0.856	0.857	0.870	0.738	0.778	0.890	0.922	0.948	1.006
Li*	0.127	0.076	0.117	0.138	0.119	0.029	0.010	0.017	0.000
Ca	0.025	0.022	0.024	0.029	0.026	0.037	0.050	0.053	0.063
Na	0.693	0.642	0.681	0.693	0.669	0.623	0.699	0.675	0.683
K	0.037	0.021	0.016	0.056	0.013	0.009	0.010	0.011	0.015
ΣX	0.756	0.685	0.722	0.778	0.708	0.669	0.760	0.739	0.762
F	0.354	0.254	0.361	0.333	0.266	0.195	0.314	0.334	0.321
Cl	0.020	0.004	0.004	0.048	0.008	0.001	0.002	0.000	0.004
OH*	0.626	0.742	0.635	0.619	0.726	0.804	0.684	0.666	0.675

Structural formula recalculated after Hawthorne and Henry (1999); *Li = 15-Σ(T + Z + Y) and OH* = OH + F + Cl = 1.

3.3.4. Mineral chemistry

Table 3 shows tourmaline analyses of the core zone of the orbicules from LR and EH granites normalized to 29 (O,OH,F,Cl); this normalization anion number was used instead of 31 oxygens (Hawthorne and Henry, 1999), in order to ease comparison with published data; accordingly, it was assumed that boron saturated the maximum allowed stoichiometry of 3000 a.p.f.u. (Yavuz et al., 2002).

Tourmalines of both localities (LR and EH) are typically high in FeO (10.5–11.7 wt %) and low in MgO (3.0–4.0 wt %), with a Fe/Mg ratio variable between 1.6 and 2.1. Li computed using the Hawthorne and Henry (1999) equation [Li = 15-(T + Z + Y)], ranges from 0 to 0.14 a.p.f.u. Schorl from LR shows a weak enrichment in Ti and Li, with lower contents of Mn, Fe and Mg, though preserving a similar Fe/Mg ratio as in the EH schorl.

According to mineral chemistry and parameters of Hawthorne

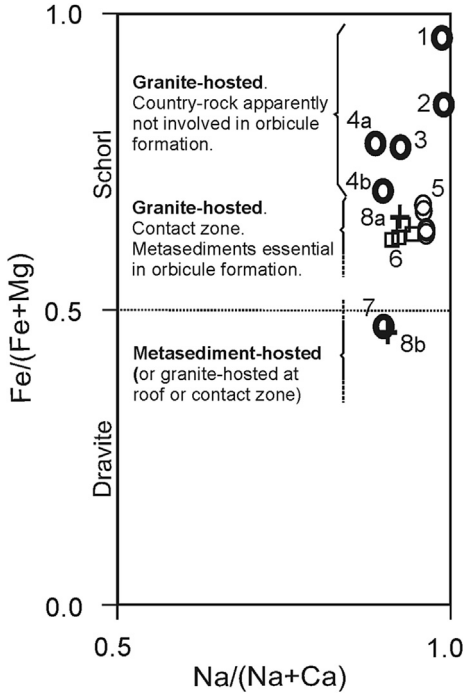

Fig. 7. Fe/(Fe + Mg) vs. Na/(Na + Ca) ratios of schorl from Los Riojanos (5) and El Hornito (6) orbicules, compared to ratios of the series schorl-dravite of orbicules from the Seagull batholith (1), Cape Granite Suite (2,3,7), Scrubber Granite (4a = zoned crystal average, 4b = unzoned crystals average), and the Moslavačka Gora granite of Croatia (8a = average of two nodule cores, 8b = average of two nodule rims, analyses 6–7 and 8–9, respectively, from Balen and Broska, 2011). Cations were normalized to 29(O,OH,F,Cl) instead of 31(O,OH,F,Cl), solely to be able to establish comparisons with older published data.

and Henry (1999), analyzed tourmalines belong to the alkaline group with Na + K values within the range 0.63–0.75. Considering their F contents and assuming full occupancy of the halogens site (OH = 1), they belong to the OH-rich subgroup; being Fe the dominant cation in the X site, the species grown in the orbicules is schorl.

In the ternary diagram of Henry and Guidotti (1985), where substitutional schemes between Fe_T-Ca-Mg and Fe_T-Al-Mg relate mineral composition with whole country rock composition, orbicular schorl reveals its affinity with field 2 of *Li-poor granitoids, pegmatites and aplites*; the same compositional field includes tourmaline from the Seagull Batholith, Haelkral and Kuils River from the Cape Granite Suite, South Africa (Sinclair and Richardson, 1992; Rozendaal and Bruwer, 1995) and the Scrubber Granite of Western Australia (Shewfelt, 2005); the exception is tourmaline from Rooiberg (Cape Granite Suite) that plots in field 6 that represents *Ca-poor, Fe-rich metapelites*, the lithologies where the orbicules are hosted.

The Na/(Na + Ca) and Fe/(Fe + Mg) ratios of schorl from both LR and EH orbicules vary from 0.95 to 0.97 and 0.62 to 0.67, respectively (Fig. 7); the #Fe values are substantially lower than those of tourmalines from Seagull, Haelkral and Kuils River, which show #Fe > 0.75, and also lower than the Fe/(Fe + Mg) ratios of those from the Scrubber Granite which are richer in Ca. Fig. 7 also shows a tendency of molar dravite enrichment toward orbicular tourmaline that crystallized close to the contact or within metasedimentary country-rocks. Alkalis and Ca variations in the X-site, particularly the weak enrichment in Na of the Los Riojanos tourmalines (#Na = 0.96 to 0.97), could be related to the Ab-rich magmatic plagioclase they replace ($An_{2\text{-}13}$ for LR and $An_{2.5\text{-}11}$for EH). Concordantly, the computed Li* in schorl from LR monzoleucogranite evidences a higher differentiation degree.

Surprisingly, analyzed core to rim profiles of the earliest schorl crystals, show compositional homogeneity, an abnormal or infrequent fact for late magmatic-, hydrothermally grown-schorl. London (1999) refers to the marked compositional oscillatory zoning in tourmaline supergroup minerals grown in open system, such as tourmaline from breccia pipes, due to thermodynamic, fluid composition, pressure and temperature changes during crystallization. A later, though scarce generation of tourmaline, evident as narrow bluish rims on schorl and also as fibrous aggregates (not analyzed), could reflect Al enrichment (Deer et al., 1992; Sinclair and Richardson, 1992).

3.3.5. Mass balance

Mass balance computations were applied to the tourmalinization process; mineral reactions between the protholithic host granite and each of both zones of the orbicules were evaluated. Gains and losses of major and trace elements were tested after various methodologies (Gresens, 1967; Grant, 1986; MacLean and Kranidiotis, 1987; MacLean, 1990; Leitch and Lentz, 1994). Table 1 shows analytical data from the unaltered protholithic

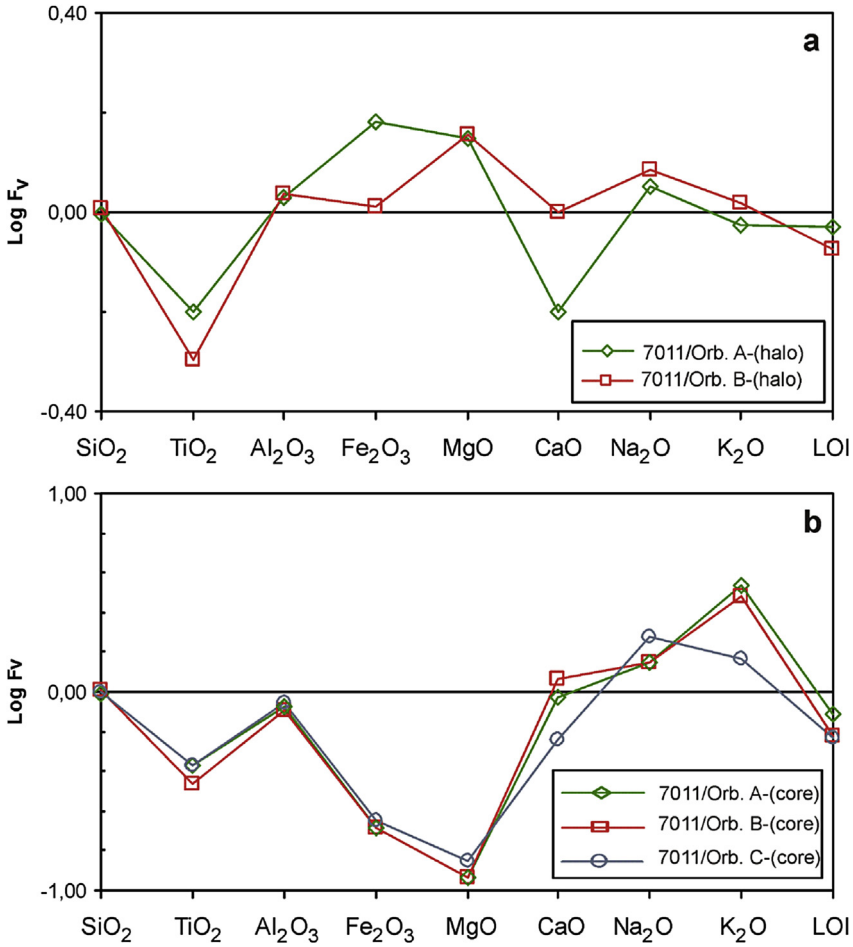

Fig. 8. Variation of volumetric factor in log units (Log F_V) for major oxide elements and LOI values. **a**. Interaction between leucogranite (sample 7011) and felsic halo, **b**. Interaction between leucogranite (same sample) and schorl-rich core (computations after Gresens, 1967).

leucogranite and both concentric zones of orbicules (felsic and melanocratic haloes); sample 7011 is compositionally representative of the LR leucogranite, which, for computational purposes is assumed to be homogeneous in the vicinities of the orbicule-rich areas.

Volume-composition diagrams (Fv-Xn) were computed after Gresens (1967) equation to evaluate reactions between the leucogranite and the leucocratic rim and the schorl-rich core. SiO_2 behaves as a relatively immobile compound with Fv = 1; Xn = 0, which slope is controlled by the oxide concentration. The ΔV for each reaction was computed as an average value of those Fv's close to unity (Fig. 8); this figure depicts the Log Fv for each oxide, placing all immobile or relatively immobile components on or close to the Log Fv = 0 line. Moving away from this line is evidence of increasing mobility within the system with positive values for volume increase and negative values for volume loss. Considering the reaction leucogranite-felsic rim, SiO_2, Al_2O_3, and K_2O are the less mobile compounds, whereas for the reaction leucogranite-melanocratic core, SiO_2, Al_2O_3, and eventually CaO, are the less mobilized oxides.

The Fv value got for the pair protolith-leucocratic rim varies between 1.033 and 1.034, which indicates a volume increase of ≈3.5% during the formation of the quartz-rich halo. The Fv value for the pair protolith-schorl rich core varies from 0.927 to 0.992, which suggests a loss of volume variable from 1 to ≈7% during the process of core tourmalinization; similar Fv values between 5 and 8.4% were found by Rozendaal and Bruwer (1995) for granite-core reactions of the Haelkraal, Kuils River and Durbanville orbicules. These volume changes are minimal, nearly isovolumetric.

The gains and losses between protolithic leucogranite and felsic rim and protolithic leucogranite-schorl-rich core from Los Riojanos are expressed as the following balanced reactions:

A) Protolith − orbicules (quartz-rich leucocratic halo, LH):

- 100 g leucogranite + 2.82 g SiO_2 + 0.05 g TiO_2 + 0.24 gr CaO + 0.42 g K_2O + 0.12 LOI ↔ 102.54 gr orbicule A-LH + 0.49 g Al_2O_3 + 0.31 gr Fe_2O_3 + 0.04 g MgO + 0.28 gr Na_2O.
- 100 g leucogranite +1.32 g SiO_2 + 0.09 g TiO_2 + 0.01 g Fe_2O_3 + 0.01 g CaO +0.25 LOI ↔ 100.34 g orbicule B-LH + 0.73 g Al_2O_3 + 0.04 g MgO +0.53 g Na_2O+ 0.05 g K_2O.

B) Protolith − orbicules (schorl-rich melanocratic core, MC).

- 100 g leucogranite + 0.10 g TiO_2 + 1.60 g Al_2O_3 + 3.42 g Fe_2O_3 + 0.97 g MgO + 0.21 LOI ↔ 96.39 g orbicule A-MC + 5.41 g SiO_2 + 0.01 g CaO + 1.16 g Na_2O + 3.33 g K_2O.
- 100 g leucogranite +0.16 g TiO_2 + 3.16 g Al_2O_3 + 3.77 g Fe_2O_3 + 1.06 g MgO +0.75 LOI ↔ 103.17 g orbicule B-MC + 1.56 g SiO_2 + 0.05 g CaO +1.05 g Na_2O+ 3.07 g K_2O.
- 100 g leucogranite +0.10 g TiO_2 + 1.04 g Al_2O_3 + 3.13 g Fe_2O_3 + 0.80 g MgO +0.24 g CaO +0.67 LOI ↔ 97.93 g orbicule C-MC + 4.69 g SiO_2 + 1.73 g Na_2O + 1.63 g K_2O.

Fig. 9 represents gains and losses of mass (g/100 g) of rock in halo-, and core-leucogranite reactions; the components K_2O, SiO_2, CaO and LOI were gained in the leucocratic halo (Fig. 9a), mostly composed of quartz, muscovite and subordinated calcite; losses of Al_2O_3, Fe_2O_3 and Na_2O in the leucocratic halo encompasses breakdown of magmatic plagioclase, Fe-Ti oxides and minor biotite. The orbicule cores (Fig. 9b) have gained Al_2O_3, Fe_2O_3, MgO and LOI, components that evidence schorl formation; a smaller gain in TiO_2 reflects rutile formation in the core. Alkalis and silica loss respond to albitic plagioclase and K-feldspar strong replacement after schorl formation.

The use of immobility tests for compatible and/or incompatible elements in binary diagrams following the criteria of MacLean and

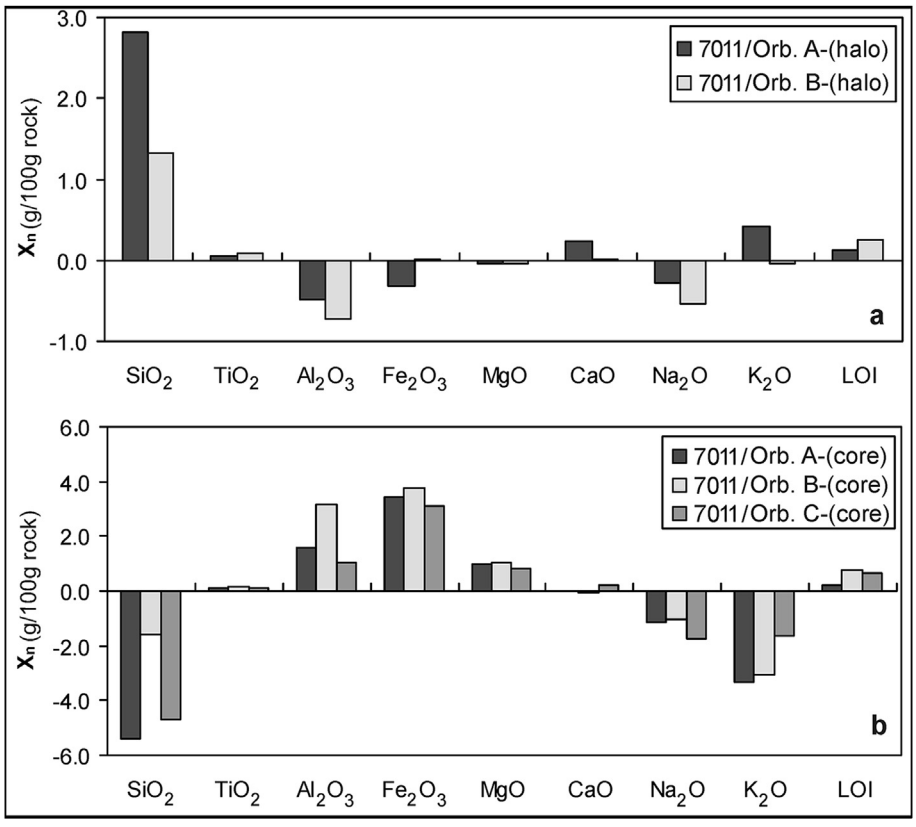

Fig. 9. Mass variation (X_n) in g/100 g of rock with gains and losses of major element oxides and volatiles (LOI) in leucogranite-halo (**a**) and leucogranite-core (**b**) reactions.

Table 4
Reconstituted composition of haloes and cores of orbicules based on an anhydrous protholithic basis and assuming immobility of SiO_2 (computed after MacLean and Kranidiotis, 1987).

Wt. %	LR0 Leucogr	Orbicule A		Orbicule B		Orbicule C
		Halo	Core	Halo	Core	Core
SiO_2	75.42	75.42	75.42	75.42	75.42	75.42
TiO_2	0.09	0.14	0.20	0.17	0.25	0.20
Al_2O_3	14.61	13.60	17.49	13.64	18.19	16.71
Fe_2O_3	0.99	0.65	4.79	0.98	4.90	4.43
MgO	0.14	0.10	1.21	0.10	1.23	1.01
CaO	0.37	0.59	0.39	0.38	0.33	0.66
Na_2O	3.51	3.11	2.52	2.92	2.50	1.87
K_2O	4.59	4.83	1.32	4.46	1.52	3.14
P_2O_5	0.28	0.4	0.23	0.26	0.17	0.28
ppm						
Zr	43	123	111	122	109	89
Y	11	43	27	39	27	24
Nb	50	29	8	28	10	10
Sr	16	46	31	54	33	40
Ba	54	239	84	269	121	101
Rb	603	333	94	278	99	351

Kranidiotis (1987) and MacLean (90) failed to demonstrate immobility, as none of them defined a regression line to the origin. Table 4 shows the reconstituted composition of the orbicules after MacLean and Kranidiotis (1987), working on an anhydrous base (LOI subtracted) and SiO_2 inmobile component (Fv = 1; Xn = 0), as was indicated by the application of the Fv-Xn Gresens equation; alumina was not considered immobile in this geochemical system due to reported evidence of Al solubility under the presence of B-rich aqueous fluids (London, 1997). Comparatively, mass changes are similar to those obtained through Gresens (1967; Table 5).

Gains and losses were also estimated using the isocon procedure (Grant, 1996; Fig. 10) that confirms the immobility of SiO_2 during orbicule formation, which plots along the line of constant volume, and so does K_2O in the felsic halo; Fig. 10 shows in the core the element oxides and traces that have been gained (Fe_2O_3, Al_2O_3,MgO, TiO_2, Ba, Sr, Y and Zr) and lost (Na_2O, K_2O, Rb and Nb); the oxides and traces gained in the halo are K_2O, Ba, Sr, Y, Zr and locally CaO, and those lost are Fe_2O_3, MgO, Na_2O, Al_2O_3, Rb and Nb. The significant increase of Ba and Sr during the generation of the felsic halo could be related to muscovitization of plagioclase where neoformed muscovite could host Ba and secondary patchy calcite could retain Sr.

In the core of the orbicules, the enrichment of Fe_2O_3, MgO and Al_2O_3 evidences schorl formation at expenses of K-feldspar consumption, represented by K_2O and Rb loss. The increase of LOI values in the cores is likely explained by B_2O_3 and (OH-) involved in tourmaline formation.

Mass balance constraints indicate that the schorl-rich core formation does not represent element redistribution in a closed system; elements gained in their cores such as Fe_2O_3, MgO and TiO_2, in abundance enough to form modal concentrations above 80% volume of schorl, need to involve an external source. Evidence of elements that could have entered into the system from an external source, other than magmatic-hydrothermal, are the anomalous contents of Zn (70–100 ppm), and also V (82–121 ppm) in country rock gneisses and schists (Table 1); Zn is up to ~3 and V up to ~100 times-enriched in the schorl-rich core with respect to the host leucogranite, and as much as 1.5 to 3 times more than country rock gneisses and schists (we lack data for these elements in the haloes). Ba, and to a lesser degree Sr enrichments in the haloes, would also need a country rock input, where both elements are much higher concentrated than in leucogranite (~8–12 and 8–9 times, respectively).

3.3.6. Fluid inclusions

Fluid inclusion microthermometric measurements were done on quartz and a few in schorl from Los Riojanos orbicules. Fluid inclusion petrographic classification was done following traditional

Table 5
Gains and losses of major and selected trace elements across zones of orbicules A, B and C, assuming SiO_2 as immobile (computed after Gresens, 1967).

Wt.%	A		B		C
	Halo	Core	Halo	Core	Core
TiO_2	0.05	0.12	0.09	0.17	0.12
Al_2O_3	−1.01	2.88	−0.97	3.58	2.10
Fe_2O_3	−0.34	3.80	−0.01	3.91	3.44
MgO	−0.04	1.06	−0.04	1.09	0.87
CaO	0.22	0.02	0.01	−0.04	0.29
Na_2O	−0.40	−0.99	−0.59	−1.01	−1.63
K_2O	0.24	−3.27	−0.13	−3.07	−1.45
P_2O_5	0.12	−0.05	−0.02	−0.11	−0.01
ppm					
Zr	80	68	79	66	46
Y	32	16	28	16	13
Nb	−21	−42	−22	−40	−40
Sr	30	15	38	17	24
Ba	185	30	215	67	47
Rb	−270	−509	−325	−504	−252

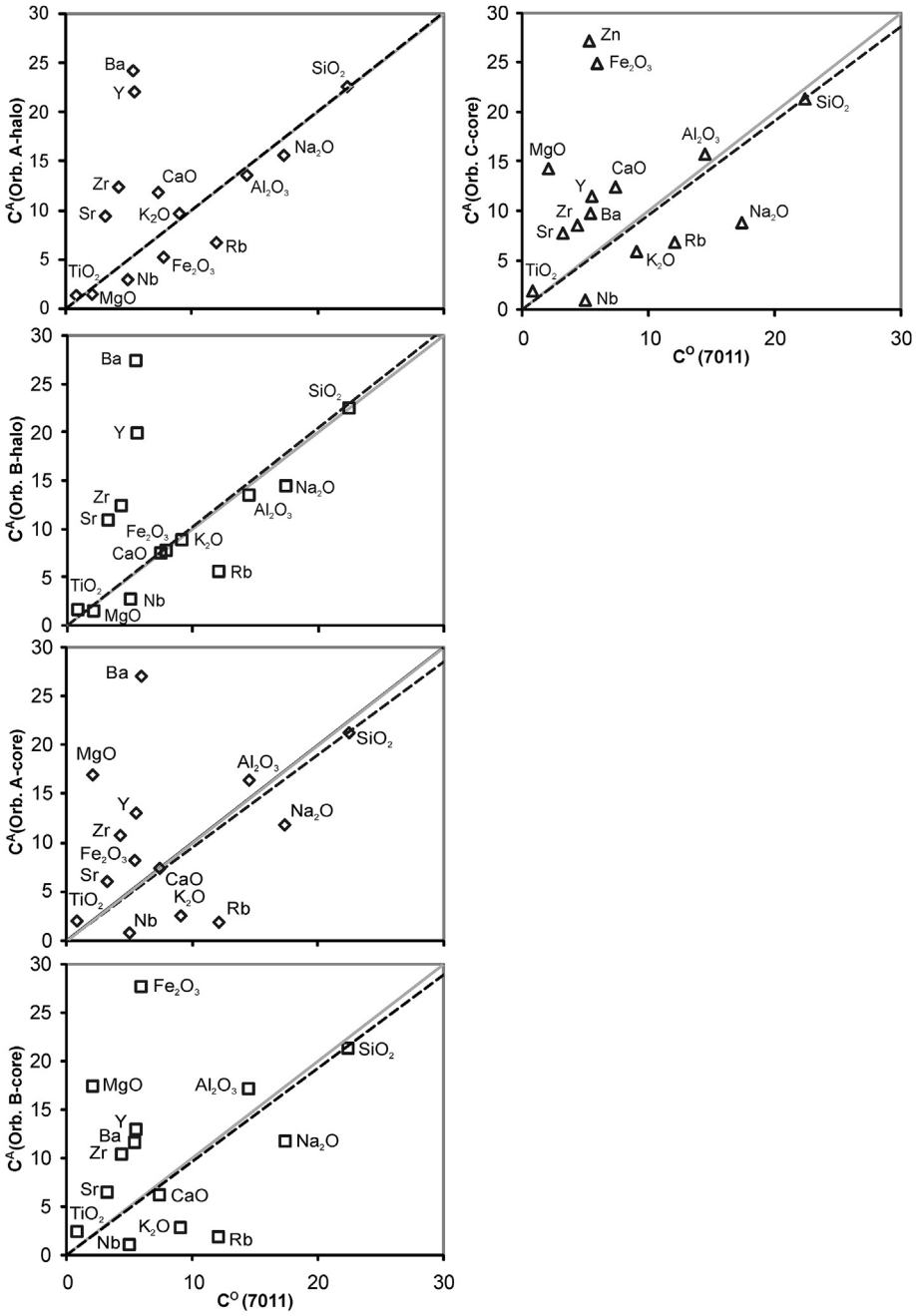

Fig. 10. Isocon graphs (Grant, 1986) of halo vs. protholith and core vs. protholith showing SiO_2 immobility and gains and losses of major and selected trace elements in orbicules A, B and C from Los Riojanos pluton; K_2O also behaves as immobile during the generation of the felsic halo. C^A = composition of the altered rock, C^O = composition of the parental rock (leucogranite, sample 7011). Data plotted in wt. % for major element oxides and in ppm for trace elements. Dashed lines = constant mass, solid lines = constant volume.

criteria (i.e., Roedder, 1984; Shepperd et al., 1985) based on phase relationships at room temperature. Six types were distinguished: type 1: quartz-hosted two phase (L + V), aqueous-, liquid-rich (F≅ 0.8–0.9) of regular morphology and sizes up to 10 μm, constant L/V ratio, isolated and also aligned along planes (Fig. 11a); type 2: quartz-, and schorl-hosted similar to type 1 but with negative crystal morphology (Fig. 11b); type 3: barely seen groups of coexistent few negative-crystal or irregular shaped fluid inclusions with intermediate degrees of filling (F≅ 0.3 to 0.8), some vapour-rich are CO_2-bearing though most ones are liquid-rich without optical evidence of CO_2; type 4: sized less than 10 μm, two phase vapour or liquid-rich (F ranging from 0.4 to 0.8), associated to planes; type 5: multiple phase (L + V + S), scarce, isolated, and of larger size than all three previous types, and type 6: monophase (only liquid), of irregular morphology with necking-down evidences.

Types 1, 2 and 3 were interpreted as of primary origin; these were found in euhedral quartz and schorl in the orbicule's core. Those classified as of type 1, following planes that do not intersect crystal borders, were considered pseudosecondary. Most measurements were taken on types 1 and 2.

Twenty measured fluid inclusions homogeneize to the liquid phase within the range ≅ 130 °C to 302 °C. Fig. 12a shows that 65% of the homogeneization temperatures (T_h) fall in the range 180–260 °C. Temperatures of the last ice crystal melting vary

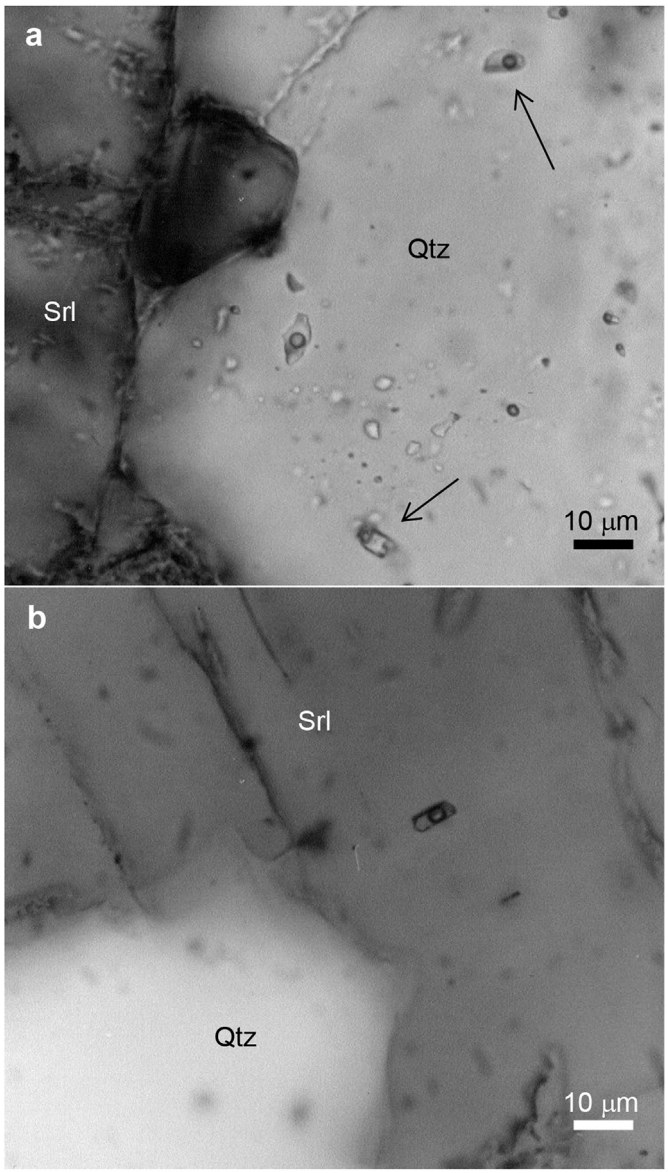

Fig. 11. Representative fluid inclusions from the Los Riojanos schorl orbicules. **a**. Type 1, primary-, two phase-, liquid-rich aqueous fluid inclusions in quartz paragenetic with schorl (distinguished with arrows from other secondary types), **b**. Primary-, negative crystal-type isolated fluid inclusion in schorl (type 2). Qtz = quartz, Srl = schorl.

from −11.3 to −0.6. These values were converted to salinities using the equation of Brown and Lamb (1989) for the system NaCl-H_2O, which yielded salinities of ~1–15 eq. wt. % NaCl. About 76% of computed values fall within the salinity range of 5–10 eq. wt. % NaCl (Fig. 12b). Fluid inclusion densities vary from 0.75 to 0.97 g/cm^3. The eutectic point coud not be observed.

A binary plot of T_h *vs.* salinity (Fig. 12c), shows that salinity decreases with decreasing temperature. This trend suggests mixing of magmatic fluids with meteoric fluids provoking dilution and thermal descent. Salinity values higher than ~7 eq. wt. % NaCl and the presence of CO_2 in type 3 inclusions suggest the involvement of a magmatic fluid component for the Los Riojanos orbicules.

If a pressure correction (Potter, 1977) is applied to a maximum T_h of 300 °C, with an average salinity of 5 eq. wt. NaCl under a maximum lithostatic pressure estimate of ~2 Kb (presence of miarolitic cavities along the pegmatitic border facies, i.e., Ragland, 1989; Candela, 1997), a ΔT of 180 °C permits to get a maximum trapping temperature of 480 °C. Isochores drawn after the Brown and Lamb (1989) equation of state, considering a ~2 kb confining pressure, yielded a trapping temperature range of 250–420 °C.

Homogenization temperatures measured in various types of fluid inclusions in quartz and tourmaline of the orbicules from the Seagull batholith, Canadá, corrected for the range 1–2 kb (Samson and Sinclair, 1992), fall in a wider range and are considerably higher in trapping temperature (300–600 °C, and as low as 150 °C); reported salinity values for the tourmalinizing fluids of the Seagull batholith range between 8 and 42 eq. wt. % NaCl + $CaCl_2$. Microthermometric studies completed by Shewfelt (2005) on tourmaline fluid inclusions from the Paleoproterozoic Scrubber Granite of the southern Gascoyne Complex in Western Australia, revealed that the nodule-forming fluid contained 14 to 15 wt % NaCl + $CaCl_2$; based on stable isotope studies and homogenization temperatures, fluid temperatures were constrained between 450 and 700 °C.

3.3.7. *Hydrogen isotopes*

The δD_{schorl} values of orbicules A and B from Los Riojanos are, respectively, −146 and −74‰ vs. SMOW; these values fall within the range of those found in granitic and haplogranitic melts. Prismatic schorl found as fan-shaped aggregates along the aplitic facies of LR pluton, between the outer pegmatite facies and the inner equigranular facies, yielded −76‰ vs. SMOW. The heaviest values are very similar as those found in the copper-rich, tourmaline-bearing Donoso breccia pipe in the giant Miocene-Pliocene Río Blanco-Los Bronces copper deposit in the Andes of central Chile (Skewes et al., 2003), where both δD and $\delta^{18}O_{schorl}$ values are dominantly magmatic with no significant input of meteoric water.

The lightest δD_{schorl} value of −146‰ (A-orbicule) could be interpreted as the result of a magmatic-exsolved fluid that exchanged with meteoric water, in a similar fashion as inferred by Dyar et al. (1999) for tourmalines of the Mount Mica pegmatite (Maine, USA), which gave δD_{schorl} values variable from −105 to −131‰.

Fractionation of hydrogen isotopes between tourmaline and water has been experimentally or empirically investigated by a few researchers (Blamart et al., 1988; Kotzer et al., 1993; Jibao and Yaqian, 1997) at different temperature ranges, and with tourmalines of different Fe/Mg compositional ratios. The equation of Kotzer et al. (1993), computed at 420 °C yielded values of $\delta D_{H20} = -45‰$ for schorl (Fe/Mg = 1.73) of the orbicule B, and of $\delta D_{H20} = -117‰$ for schorl (Fe/Mg = 1.97) of the orbicule A; the temperature used was estimated from the maximum T_h corrected for a pressure of 2.0 kbars, based on the presence of miaroles in the pegmatitic facies along the pluton western contact, and on thermobarometric data from contact metamorphism of the Achala batholith (Baldo and Verdecchia, 2014), who interpreted an emplacement of <2.5 kbars. The above computed D/H ratios suggest a pure magmatic origin for orbicule A and a mixed origin of interaction of magmatic with meteoric fluids for orbicule B.

3.3.8. *Formation conditions of orbicules*

Boron is an incompatible element in igneous systems. It is characteristic of S-type, highly fractionated peraluminous systems (ASI >1.2); concentrations of 1–4 wt % B_2O_3 are common in evolved peraluminous systems, where it lowers the viscosity and favors felsic melt migration (Manning, 1981; Bernard et al., 1985; London, 1992, 1999). Tourmaline stability is not only controlled by B_2O_3 availability, but also by temperature, pressure, and Na-, Fe-, Al-, Si-, and OH-activity. If F is present, its increasing content also raises the minimum B content needed to reach saturation which is normally 2 wt % B_2O_5 (London, 1992, 1999). The scarcity of Fe and Mg in felsic melts also affects tourmaline formation, being sometimes the unique source of such elements the breakdown of biotite (Bernard

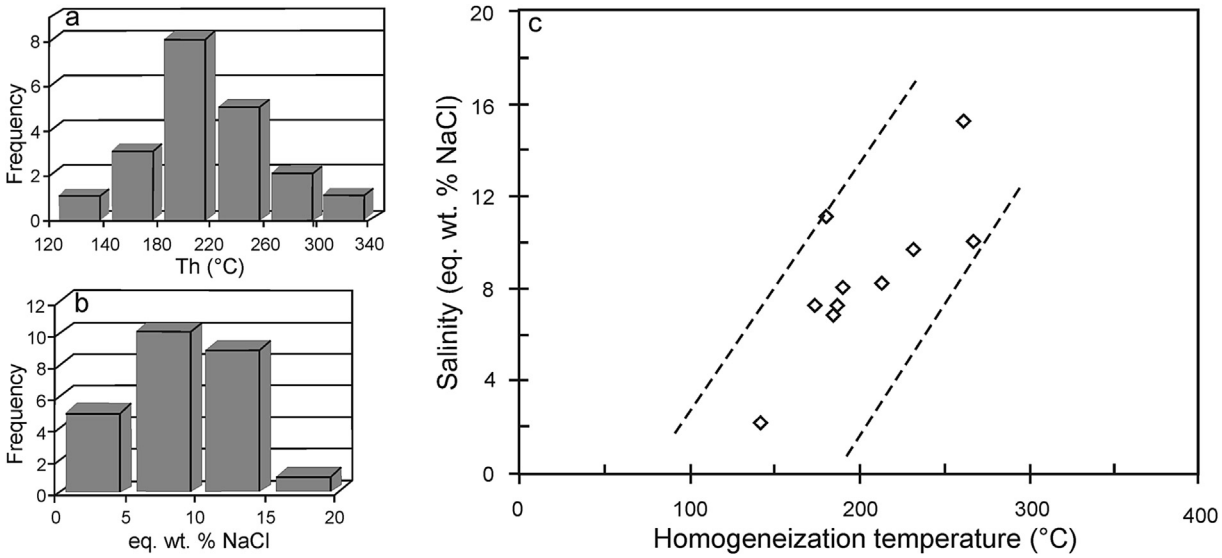

Fig. 12. Homogenization temperatures (**a**) and salinity estimates (**b**) histograms from primary fluid inclusions in quartz and schorl; **c**. Homogenization temperature vs. salinity plot showing a fluid mixing trend ($r^2 = 0.62$).

et al., 1985; Wolf and London, 1997; London, 1997, 1999). As long as crystallization proceeds, boron partitions preferentially into the exsolved fluid phase and concentrates in late to postmagmatic stages (London, 1999).

In the LR leucogranite, the formation of tourmaline was probably delayed to late to postmagmatic stages, probably due to a control exerted by the low availability of Fe and Mg (biotite < 2 vol %) at the initial stage of B exsolution, and also due to F enrichment of the melt (Dorais et al., 1997), which could also have needed > 2 wt % B_2O_3 to crystallize schorl. The high diffusivity of B allowed consumption of the scarcely available Fe and Mg of the leucogranitic source and, principally, from contacting biotite-rich gneiss roof pendants.

Known hypothesis on the origin of tourmaline orbicules developed in the apical portions of intrusive bodies are diverse. Some consider a hydrothermal replacement of previously crystallized granite (e.g., Brammall and Harwood, 1925; Rozendaal and Bruwer, 1995); other researchers invoke the separation or exsolution and trapping of B-rich fluids coexisting with the granite melt (e.g., Sinclair and Richardson, 1992; Shewfelt, 2005), and some of the most recent interpretations explain their origin after liquid immiscibility during late stages of granitic melt crystallization: 1-From an immiscible Na–B–Fe-rich hydrous melt. (i.e., Trumbull et al., 2008); 2-From rapid crystallization of boron-rich silicate melt bubbles earlier separated from the acidic magma before final emplacement (i.e., Dini, 2011); 3- After a late-stage boron-rich volatile fluid phase exsolved from crystallizing granite melt (i.e., devolatilization, Balen and Broska, 2011), 4-Through separation of an immiscible hydrous borosilicate melt from the crystallizing granitic aluminosilicate melt prior to complete crystallization of biotite to allow Fe and Mg a preferential partition into the B-rich melt (i.e., Drivenes et al., 2015).

In the LR leucogranite boron was likely concentrated by exsolution into the vapour phase after fractional crystallization (e.g., London, 1999). Fe and Mg have been majoritarily supplied by biotite-rich metasedimentary roof pendants, as supported by mass balance computations that show gains of Fe, Mg and Ti during the schorl-rich core growth; gains of trace elements such as Zn, V, probably Pb, Ba and Sr are also indicated by mass balance as provided by a non-granitic external source. Zn (and Pb) capture, movilization and transport, like it occurs with Sn and W in other world occurrences, were likely favored by the high diffusivity of B^-.

The morphology of orbicules and their restricted location in the cupola of the pluton within the contact zone with the country-rock metasediments, likely suggest that boron-rich aqueous fluids were trapped like ascending bubbles during Los Riojanos melt

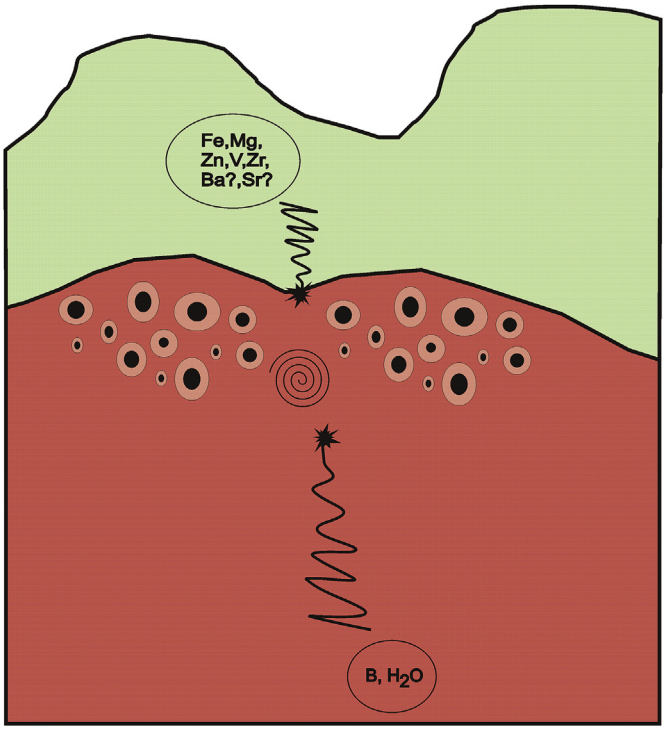

Fig. 13. Cartoon depicting schorl orbicule formation at the contact zone between underlying leucogranite and metasedimentary country-rock. The spiral symbolizes the confined reaction zone (chemical gains and losses) where orbicules are formed within crystallized leucogranite. The descending path represents elements added from biotite-rich metasedimentary country rocks, whereas the path pointing upwards represents ascending boron-rich, aqueous fluids exsolved from leucogranite melt.

crystallization (Fig. 13). The homogeneous composition of core schorl crystals suggest stable conditions during crystallization, probably favored by fast nucleation-growth and the high diffusion of the fluid. When B_2O_3 is > 2 wt %, schorl feeds first from K-spar and after that from plagioclase, relying on Fe and Mg availability removed from granitic and/or metamorphic biotite after fluid-rock interaction. The outer rim of orbicules is devoid of biotite, *per se* scarce in the leucogranite, which is likely explained by Fe and Mg deficiency caused by the earlier capture of these elements by the boron-rich phase in the core. Plagioclase alteration to muscovite (sericite) controls K availability in the system through coupled reactions (K released from tourmaline replacement of K-feldspar substitutes for Na^+ or Ca^{2+}); neoformation of sericite in the anorthite-richer core of plagioclase releases Ca^{2+} that might crystallize as calcite.

Tourmaline formation at the expenses of K-feldspar and plagioclase required a provision of Fe, Mg and Al, the release of Si (precipitated as quartz), and of Na and K. The origin of the subhedral-euhedral quartz within the felsic halo is not completely understood, though it more likely precipitated from the fluid migrated outward from core reactions. Even none of several tenths of observed orbicules from Los Riojanos developed miarolitic cavities or proto-miaroles, the development of a subhedral-euhedral mosaic of secondary quartz intergrown with subhedral schorl, and the presence of thin overgrown rims of more evolved tourmaline on schorl are suggestive of a tendency to miarole formation; however, the small loss of volume after core reactions do not support this tendency.

Analyzed profiles from core to rim of earliest schorl crystals show compositional homogeneity, suggesting at least closed–system conditions of crystallization in the core of orbicules, an abnormal or infrequent fact for postmagmatic-, hydrothermally-grown schorl; London (1999) refers to the marked compositional oscillatory zonation in tourmaline grown in open system conditions. The increase of LOI values in the core is likely explained by B_2O_3 and (OH-) involved in tourmaline formation, which increases Al solubility in the residual magmatic fluid.

The existence of anomalous contents of Zn, V and Pb in the core of the orbicules of Los Riojanos, where tourmaline dominates volumetrically, evidences their concentration in schorl, in the absence of other minerals capable of accommodating these elements. In general, highly evolved peraluminous systems tend to concentrate elements such as Sn and W, and Zn–Pb subordinately (e.g., Newberry et al., 1990; Strong, 1994). Tin and tungsten occur in very low concentrations in both LR leucogranite and in the orbicules, and the lack of known Zn and Pb mineralizations within the leucogranite and nearby country rock support a limited availability of these metallic elements in the system.

Trace elements in whole rock analyses of gneisses from the immediate vicinity of orbicules location in Los Riojanos yielded anomalous concentrations of Zn, V and Pb, and also of Ba and Sr (Table 1). These amphibolite facies metasediments of the Neoproterozoic-Cambrian Complejo Metamórfico San Carlos (Gaido et al., 2005) were very likely the source of base metals and V in the schorl orbicules. In this scenario, the metasedimentary country rocks not only were sources of Fe and Mg, but also of other cations. Akçay et al. (1995) explained tourmaline composition of a Sb-Hg ± W mineralization in Central Turkey as the consequence of interaction of postmagmatic tourmaline-forming fluids with metamorphic host lithologies. Cempírek et al. (2013) found high concentrations of V, Cr and Ti (as well as elevated Mn, Zn, Sc, Sn, and Sr) in oxy-dravite to dravite in graphite quartzites overprinted by a high-grade metamorphic event, most probably as a result of hydrothermal dissolution of (Ti,V)-oxides (rutile) and other quartzite accessory phases.

In the same line of evidence, Balen and Broska (2011) concluded that a significant influx of fluid derived from wallrock mixed with the fluid phase from the residual melt of the Moslavačka Gora granite in Croatia, which increased the dravite molar content in nodular tourmaline respect of disseminated, molar schorl-richer magmatic tourmaline. We did not find orbicules hosted in the metasediments, however, Rozendaal and Bruwer (1995) found dravite orbicules hosted in the metapelitic country rocks of Rooiberg, which compositions reflected the Ca-poor nature of the metasediments. LR and EH schorl also shows a tendency of molar dravite enrichment (Fig. 8), with intermediate Fe/(Fe + Mg) ratios between granite-, and metapelite-hosted orbicules, which is interpreted to reflect the strong influence of fluid-metasediment rock interaction.

The δD_{schorl} values of orbicules from Los Riojanos (−74 and −146‰ *vs.* SMOW, respectively) are representative of those found in granitic and haplogranitic melts. δD_{H20} computed at 420 °C (T_h corrected for a pressure of 2.0 kbars), yielded values of −45‰ for schorl of the orbicule B, and of $\delta D_{H20} = -117‰$ for schorl of the orbicule A; these computed D/H ratios suggest a pure magmatic origin for fluid of orbicule A and a mixed origin of interaction of magmatic with meteoric fluids for orbicule B. The low salinities registered from fluid inclusion data (5–7 eq. wt. % NaCl) also support a diluted magmatic fluid. Likely, the epizonal emplacement of LR pluton might have allowed the interaction of a magmatic B-rich exsolved phase with percolating descending meteoric waters through the metasedimentary country rock. The presence of CO_2 in scarcely found fluid inclusions within the same population of primary-, H_2O-rich ones of higher salinity suggest a stronger influence of the magmatic source.

In general, this contribution supports the late-magmatic exsolved-fluids scenario for the formation of orbicules as proposed by earlier researchers worldwide (e.g., Shewfelt, 2005; Balen and Broska, 2011), and does not suggest any arguments against liquid immiscibility at earlier stages prior to aqueous-, boron-rich fluids exsolution from melt. In the particular study case of Los Riojanos, some data prevents from accepting a magmatic origin derived directly from immiscible melts: 1- The lack of disequilibrium textures between earlier-crystallized granitic feldspars and neoformed “magmatic” schorl, and the presence, in our opinion, of typical metasomatic-hydrothermal replacement textures, 2- The relatively low temperature and low salinity values estimated from fluid inclusion data, 3- The D/H ratios computed at fluid inclusion trapping temperatures that suggest a magmatic-hydrothermal and mixed magmatic-meteoric origin for the fluids, 4- Mass balance computations that indicate that elements such as Fe, Mg and other metallic traces, specially Zn and V, can only be explained if metasedimentary country rocks are involved as the major source of those elements, otherwise schorl formation would have not been viable, 5- Fluid-rock interaction between the host leucogranite and a late tourmalinizing fluid is supported by the range of values of the T_3 tetrad effect.

Field evidence favors this interpretation because thousands of tourmaline orbicules are concentrated along the contact zone of the granite cupola and wall rock or large roof-pendants, being absent elsewhere throughout the pluton; the irregular distribution seen today could be due to more than one factor, among them, different topographic levels might show different erosive levels, or, more likely, boron exsolution and upward diffusivity could have been non-uniform throughout the granite cupola. Shewfelt (2005) proposed the formation of the tourmaline nodules of the Scrubber Granite from Western Australia as the result of the rise of buoyant pockets or bubbles of volatile fluid exsolved from the crystallizing Scrubber Granite magma at depth; she assigned the wide variation of orbicule morphology to different vertical levels of orbicule

crystallization within the vapour saturation zone, being the "rosette" and "spherical" morphologies the highest-crystallized types; the fact that miarolitic types were not found in the Scrubber Granite might indicate that confining pressures were somewhat higher than 2 kbars. Nevertheless, Perugini and Poli (2007) arrived to a different conclusion regarding the degree of irregularity of nodules from the Capo Bianco aplite in the Elba Island; these authors performed morphometric analyses where orbicules are analogs of fractals and their growth after numerical simulations was performed by applying a Diffusion-Limited Aggregation process. The different morphologies of nodules, especially between the rounded and dendritic types, were explained by considering a chaotic magmatic system with a complex interplay between growth rate in different dynamical regions, latent heat of crystallization, and local convection dynamics.

The latest stage of orbicule growth in our study case could be represented by crystallization of rims of bluish tourmaline overgrown on earlier schorl, and fibrous tourmaline included in subhedral-euhedral quartz and in partially replaced feldspars. Similar occurrences of late blue tourmaline overgrowths assigned to a magmatic exsolved-fluid have also been studied by means of B-isotopes by Trumbull et al. (2008) and reported as of foititic composition by Drivenes et al. (2015).

4. Conclusions

Schorl-rich orbicules are found in at least seven localities of central and northwestern Argentina. The intrusive bodies that host tourmaline orbicules are peraluminous S- and A-type granites that belong to the Famatinian Orogeny of Ordovician age and the Achalian magmatism of Devonian age. Field occurrence, petrographic data and mineral chemistry does not practically differ from other worldwide occurrences reported by previous researchers. Another remarkable analogy among worldwide occurrences is the orbicule crystallization level restricted to the apical, cupola zone of strongly fractionated granites close to the contact with enclosing country-rocks; the transition from non-miarolitic to proto-miarolitic and miarolitic orbicules suggests that formation is favored in epizonal intrusives emplaced at ~2 kbars. The genesis of orbicules from the LR leucogranite in the Achala Batholith can be explained by fluid-rock interaction between fluids exsolved from a hydrous-, boron-rich melt and previously crystallized granitic melt. Independently of the favored genetic hypothesis, the mechanism that separated boron was extremely effective to raise its concentration from 100- to 300-fold its original content in the leucogranite melt. Mass balance of major and selected trace elements suggest that schorl from the core of the orbicules could have hardly formed without elements gained from metasedimentary country-rock provenance such as Fe and Mg (±Zn, V, Pb, Ba, Sr, LREE). Other evidence that supports fluid-rock interaction between crystallized leucogranite and an aqueous-rich exsolved-fluid are the replacement textures of microcline and plagioclase by schorl, the relatively low temperature and diluted salinities from trapped fluid inclusions in schorl and paragenetic quartz, the δD_{H2O} signatures that range from magmatic-hydrothermal to mixed magmatic-meteoric water, and the behavior of the T_3 REE segment.

Acknowledgments

Schorl microanalyses were acquired by RL with the help of Dr. M.J. Dorais at Bringham Young University, Provo, Utah; plagioclase and mica analyses were obtained with the aid of Dr. A.B. Guereschi at the LAMARX, Universidad Nacional de Córdoba, Argentina. Hydrogen isotope analyses were run by A. Sarkar at the Stable Isotope Lab of Indiana University at Bloomington, Indiana. A. Dini kindly sent us reprints of papers of his authorship. This work was supported with grants from Secretaría de Ciencia y Técnica de la Universidad Nacional de Córdoba (Res. 203/14 to RL), and PIP 2013–2015 GI, Code 11220120100554, from the Consejo Nacional de Investigaciones Científicas y Técnicas de la República Argentina (112 201201 00298) to M.A. Galliski. F. Cecenarro, F. Colombo, G. Cuello, J. Elortegui Palacios and F. Parra, kindly contributed photographies and some descriptive data of schorl orbicules from northwestern argentinian localities. M.E. Biglia, C. Bossio and M.J. Espeche helped with drafting. We acknowledge the remarks of two anonymous reviewers and the editorial handling of Dr. Víctor Ramos.

References

Akagi, T., Nakai, S., Masuda, A., 1994. The Tetrad Effect, a General Effect in Partitioning of REE between Aqua and Solid. Goldschmidt Conference, Edinburgh, pp. 7–8.
Akçay, M., Moon, C.J., Scott, B.C., 1995. Fluid inclusions and chemistry of tourmalines from the Gümüþler Sb-Hg ± W deposits of the Niðde massif (Central Turkey). Chem. Erde 55, 225–236.
Baldo, E.G., Verdecchia, S.O., 2014. Las metamorfitas de contacto asociadas al magmatismo achaliano de las Sierras de Córdoba. In: Martino, R.D., Guereschi, A.B. (Eds.), Geología y Recursos Naturales de la provincia de Córdoba, Relatorio del XIX Gongreso Geológico Argentino, pp. 349–363.
Balen, D., Broska, I., 2011. Tourmaline nodules: products of devolatilization within the final evolutionary stage of granitic melt? In: Sial, A.N., Bettencourt, J.S., De Campos, C.P., Ferreira, V.P. (Eds.), Granite-related Ore Deposits, vol. 350. Geological Society of London Special Publication, pp. 53–68.
Balen, D., Petrinec, Z., 2011. Contrasting tourmaline types from peraluminous granites: a case study from Moslavačka Gora (Croatia). Mineralogy Petrology 102, 117–134.
Bernard, F., Moutou, P., Pichavant, M., 1985. Phase relations of leucogranites and the significance of tourmaline in silicic magmas. J. Geol. 93, 271–291.
Blamart, D., Pichavant, M., Sheppard, S.M.F., 1988. D/H isotopic fractionation between tourmaline and water; the experimental calibration of tourmaline-mineral geothermometers at 500 degrees to 700 degrees C. Chem. Geol. 70 (1–2), 182.
Boudreaux, A.P., 2014. Mineralogy and Geochemistry of the Erongo Granite and Interior Quartz-tourmaline Orbicules and NYF-type Miarolitic Pegmatites, Namibia. Theses and Dissertations. University of New Orleans. Paper 1854 (USA).
Boynton, N.V., 1984. Cosmochemistry of the rare earth elements: meteorite studies. In: Henderson, P. (Ed.), Rare Earth Element Geochemistry, Developments in Geochemistry 2. Mineralogical Society of America, pp. 64–114.
Brammall, H., Harwood, H.F., 1925. Tourmalinization in the dartmoor granite. Mineral. Mag. 2, 319–330.
Brogioni, N., 1993. El batolito de Las Chacras-Piedras Coloradas, provincia de San Luis: geocronología Rb-Sr y ambiente tectónico. XII Congr. Geol. Argent. II Congr. Exploración Hidrocarburos 4, 54–60.
Brown, P.E., 1989. FLINCOR: A microcomputer program for the reduction and investigation of fluid-inclusion data. Am. Miner. 74, 1390–1393.
Brown, P.E., Lamb, W.M., 1989. P-V-T properties of fluids in the system H2O-CO2-NaCl: New graphical presentations and implications for fluid inclusion studies. Geochim. Cosmochim. Acta 53, 1209–1221.
Buriánek, D., Novák, M., 2003. Tourmaline orbicules in leucogranites as indicator of geochemical fractionation of late solidus to early subsolidus magmatic fluids. J. Czech Geol. Soc. 48 (1–2), 30.
Buriánek, D., Novák, M., 2004. Morphological and compositional evolution of tourmaline from nodular granite at Lavičky near Vleké Meziříči, Moldanubicum, Czech Republica. J. Czech Geol. Soc. 49 (1–2), 81–90.
Buriánek, D., Žáček, V., 2015. Compositional variations in tourmalines from peraluminous rocks of the Dipilto Granitic Batholith, Eastern Chortis Terrane, Nicaragua: tracers of magmatic to hydrothermal evolution. J. Geosciences 60, 91–112.
Candela, P.A., 1997. A review of shallow, ore-related granites: textures, volatiles, and ore metals. J. Petrology 38, 1619–1633.
Cempírek, J., Houzar, S., Novák, M., Groat, L.A., Selway, J.B., Šrein, V., 2013. Crystal structure and compositional evolution of vanadium-rich oxy-dravite from graphite quartzite at Bítovánky, Czech Republic. J. Geosciences 58, 149–162.
Colombo, F., 2007. Geología, mineralogía y génesis de granitoides de tipo A y sus pegmatitas asociadas en el plutón compuesto El Portezuelo (Granito Papachacra, provincia de Catamarca). Ph.D. Thesis. Facultad de Ciencias Exactas, Físicas y Naturales, Universidad Nacional de Córdoba, Argentina.
Deer, W.A., Howie, R.A., Zussman, J., 1992. The Rock Forming Minerals. Longman Scientific & Technical, Hong Kong.
Demange, M., Álvarez, J.O., López, L., Zarco, J., 1993. Existencia de series magmáticas diferentes en el batolito de Achala (Córdoba, Argentina). XII Congr. Geol. Argent. II Congr. Exploración Hidrocarburos 4, 23–29.
Demange, M., Álvarez, J.O., López, L., Zarco, J., 1994. Geoquímica de las biotitas del

batolito de Achala (Córdoba, Argentina): su importancia como marcadores evolutivos. II Reunión Min. Metalog., Jorn. Mineral. Petrog. y Metalog. Rocas Ultrabásicas 3, 49–55.
Demange, M., Álvarez, J.O., López, L., Zarco, J., 1996. The Achala batholith (Cordoba, Argentina): a composite intrusion made of five independent magmatic suites. Magmatic evolution and deuteric alteration. J. S. Am. Earth Sci. 9, 11–25.
Demirel, S., Göncüoĉlu, M.C., Topuz, G., Isik, V., 2009. Geology and chemical variations in tourmaline from the quartz–tourmaline breccias within the Kerkenez granite–monzonite massif, central Anatolian crystalline complex, Turkey. Can. Mineral. 47, 787–799.
Didier, J., 1973. Granites and Their Enclaves: the Bearing of Enclaves on the Origin of Granites. Elsevier, Amsterdam.
Dill, H.G., Garrido, M.M., Melcher, F., Gomez, M.C., Luna, L.I., 2012. Depth-related variation of tourmaline in the breccia pipe of the San Jorge porphyry copper deposit, Mendoza, Argentina. Ore Geol. Rev. 48, 271–277.
Dini, A., 2011. An example of fluid immiscibility during the subvolcanic emplacement of a boron-rich acidic melt: the Capo Bianco aplite (Elba Island, Italy). Goldschmidt Conf. Abstr. 762.
Dini, A., Corretti, A., Innocenti, F., Rocchi, S., Westerman, D.S., 2007. Sooty sweat stains or tourmaline spots? The Argonauts on the Island of Elba (Tuscany) and the spread of Greek trading in the Mediterranean Sea. In: Piccardi, L., Masse, W.B. (Eds.), Myth and Geology, vol. 273. Geological Society of London Special Publication, pp. 227–243.
Dorais, M.J., Lira, R., Chen, Y., 1997. Origin of biotite-apatite-rich enclaves, Achala batholith, Argentina. Contributions Mineralogy Petrology 130, 31–46.
Drivenes, K., Larsen, R.B., Müller, A., Sørensen, B.E., Wiedenbeck, M., Raanes, M.P., 2015. Late-magmatic immiscibility during batholith formation: assessment of B isotopes and trace elements in tourmaline from the Land's End granite, SW England. Contributions Mineralogy Petrology 169 (6), 56. http://dx.doi.org/10.1007/s00410-015-1151-6.
Dyar, M., Guidotti, C., Core, D., Wear, K., Wise, M., Francis, C., Johnson, K., Brady, J., Robertson, D., Cross, L., 1999. Stable isotope and crystal chemistry of tourmaline across pegmatite-country rock boundaries at Black Mountain and Mount Mica, southwestern Maine, U.S.A. Eur. J. Mineralogy 11, 281–294.
Eichenlaub, A.B., 2007. Exploration of Genetic Links between Breccia Pipes and Porphyry Copper Deposits in a Laramide Hydrothermal System, Sombrero Butte, Pinal County, Arizona. Master Thesis. Department of Geosciences, The University of Arizona.
Elortegui Palacios, J., 2011. Petrología y génesis del Granito Las Burras y rocas plutónicas asociadas (Faja Magmática Oriental), Puna jujeña. Ph.D. Thesis. Universidad Nacional de Córdoba, Argentina, 307 pp., 1 map.
Fieremans, M., De Paepe, P., 1982. Genesis of tourmalinites from Belgium: petrographical and chemical evidence. Mineral. Mag. 46, 95–102.
Gaido, M.F., Zarco, J.J., Miró, R.C., Sapp, M., Gamba, M.T., Lopez, H., 2005. Hoja geológica 3166-30: Los Gigantes, provincia de Córdoba, 1:100000. Servicio Geológico Minero Argentino, Instituto de Geología y Recursos Minerales, Buenos Aires, Argentina. Boletín 299.
Grant, J.A., 1986. The isocon diagram-A simple solution to Gresens' equation for metasomatic alteration. Econ. Geol. 81, 1976–1982.
Gresens, R.L., 1967. Composition-volume relationships of metasomatism. Chem. Geol. 2, 45–65.
Hawthorne, F.J., Henry, D.J., 1999. Classification of the minerals of the tourmaline group. Eur. J. Mineralogy 11, 201–216.
Hellingwerf, R.H., Gatedal, G., Gallagher, V., Baker, J.H., 1994. Tourmaline in the central Swedish ore district. Miner. Deposita 29, 189–205.
Henry, D.J., Dutrow, B., 2001. Compositional zoning and element partitioning in nickeloan tourmaline from a metamorphosed karst bauxite from Samos, Greece. Am. Mineralogist 86, 1130–1142.
Henry, D.J., Guidotti, C.V., 1985. Tourmaline as a petrogenetic indicator mineral: an example from the staurolite-grade metapelites of NW Maine. Am. Mineralogist 70, 1–15.
Hinsberg, V.J., van, Henry, D.J., Marschall, H.R., 2011. Tourmaline: an ideal indicator of its host environment. Can. Mineral. 49, 1–16.
Irber, W., 1999. The lanthanide tetrad effect and its correlation with K/Rb, Eu/Eu*, Sr/Eu, Y/Ho, and Zr/Hf of evolving peraluminous granite suites. Geochimica Cosmochimica Acta 63, 489–508.
Jiang, S.-Y., Palmer, M.R., Slack, J.F., Shaw, D.R., 1998. Paragenesis and chemistry of multistage tourmaline formation in the Sullivan Pb-Zn-Ag deposits, British Columbia. Econ. Geol. 93, 47–67.
Jiang, S.-Y., Yang, J.-H., Novák, M., Selway, J., 2003. Chemical and boron isotopic compositions of tourmaline from the Lavicky leucogranite. Czech Repub. Geochem. J. 37, 545–556.
Jibao, G., Yaqian, Q., 1997. Hydrogen isotope fractionation and hydrogen diffusion in the tourmaline-water system. Geochimica Cosmochimica Acta 61, 4679–4688.
King, R.W., Kerrich, R.W., Daddar, R., 1988. REE distributions in tourmaline: an INAA technique involving pretreatment by B volatization. Am. Mineralogist 73, 424–431.
Kotzer, T.G., Kyser, T.K., King, R.W., Kerrich, R., 1993. An empirical oxygen- and hydrogen-isotope geothermometer for quartz-tourmaline and tourmaline-water. Geochimica Cosmochimica Acta 57, 3421–3426.
Leitch, C.H.B., Lentz, D.R., 1994. The Gresens approach to mass balance constraints of alteration systems: methods, pitfalls, examples. Geological Association of Canada, Short Course Notes. In: Lentz, D.R. (Ed.), Alteration and Alteration Processes Associated with Ore-forming Systems, vol. 11, pp. 161–192.
Lira, R., 1985. Tipología y evolución de rocas graníticas en su relación con el hemiciclo endógeno de la geoquímica del uranio. Aspectos metalogenéticos. Sector Septentrional del Batolito de Achala, provincia de Córdoba. Ph.D. Thesis. Universidad Nacional de Córdoba, Argentina.
Lira, R., 1987. Episienitas feldespáticas y su relación con depósitos uraníferos en el batolito de Achala, provincia de Córdoba. Rev. Asoc. Geol. Argent. 42 (3–4), 388–406.
Lira, R., Galliski, M.A., Bernard, F., Roquet, M.B., 2012. The intragranitic Potrerillos NYF pegmatites and their A-type host granites of the Las Chacras – potrerillos batholith, Sierra de San Luis, Argentina. Can. Mineral. 50, 1729–1750.
Lira, R., Kirschbaum, A.M., 1990. Geochemical evolution of granites from the Achala batholith of the Sierras Pampeanas, Argentina. Geol. Soc. Am. Special Pap. 241, 67–76.
Lira, R., Ripley, E.M., Español, A.I., 1996. Meteoric water induced selvage-style greisen alteration in the Achala batholith, central Argentina. Chem. Geol. 133, 261–277.
Lira, R., Sfragulla, J., 2014. El magmatismo devónico-carbonífero: el batolito de Achala y plutones menores al norte del cerro Champaquí. In: Martino, R.D., Guereschi, A.B. (Eds.), Los Recursos Naturales de la provincia de Córdoba. Relatorio del XIX Congreso Geológico Argentino, pp. 293–347.
London, D., 1992. The application of experimental petrology to the genesis and crystallization of granitic pegmatites. Can. Mineral. 30, 499–540.
London, D., 1997. Estimating abundances of volatile and other mobile components in evolved silicic melts through mineral-melt equilibria. J. Petrology 38, 1691–1706.
London, D., 1999. Stability of tourmaline in peraluminous granite systems: the boron cycle from anatexis to hydrothermal aureoles. Eur. J. Mineralogy 11, 253–262.
London, D., 2008. Pegmatites. Can. Mineral. Spec. Publ. 10, 347.
London, D., Morgan IV, G.B., Wolf, M.B., 1996. Boron in granitic rocks and their contact aureoles. In: Grew, E.S., Anovitz, L.M. (Eds.), Boron: Mineralogy, Petrology and Geochemistry. Reviews in Mineralogy, vol. 33, pp. 299–330.
MacLean, W.H., 1990. Mass Change calculations in altered rock series. Miner. Deposita 25, 44–49.
MacLean, W.H., Kranidiotis, P., 1987. Immobile elements as monitors of mass transfer in hydrothermal alteration: Phelps Dodge massive sulfide deposit, Matagami, Quebec. Econ. Geol. 82, 951–962.
Manning, D.A., 1981. The application of the experimental studies in determining the origin of topaz-quartz-tourmaline rock and tourmaline-quartz rocks. Proc. Ussher Soc. 69, 121–127.
Masuda, A., Kawakami, O., Dohomoto, Y., Takenaka, T., 1987. Lanthanide tetrad effects in nature: two mutually opposite types, W and M. Geochem. J. 21, 119–124.
Monecke, T., Kempe, U., Monecke, J., Sala, M., Wolf, D., 2002. Tetrad effect in rare earth element distribution patterns: a method of quantification with application to rock and mineral samples from granite-related rare metal deposits. Geochimica Cosmochimica Acta 66, 1185–1196.
Montenegro, T., 2002. Geoquímica de elementos traza y tierras raras durante la episienitización, sector central del batolito de Achala, provincia de Córdoba. XV Congr. Geol. Argent. 1, 456–461.
Neiva, A.M.R., 1974. Geochemistry of tourmaline (schorlite) from granites, aplites and pegmatites from northern Portugal. Geochimica Cosmochimica Acta 38, 1307–1317.
Newberry, R.J., Burns, L.E., Swanson, S.E., Smith, T.E., 1990. Comparative petrologic evolution of the Sn and W granites of the Fairbanks-Circle area, interior Alaska. Geol. Soc. Am. Special Pap. 246, 121–142.
Ortiz Suárez, A., Grosso Cepparo, P., Gómez Figueroa, J., Erroz, M., Montenegro, T., 2009. Geología del basamento en el extremo noroeste de la Sierra de San Luis. Rev. Asoc. Geol. Argent. 64 (3), 481–492.
Ortiz Suárez, A., Ulacco, H., Ojeda, G., 1997. Geología del granito El Hornito, provincia de San Luis, Argentina. VIII Congr. Geol. Chil. 2, 1413–1417.
Perugini, D., Poli, G., 2007. Tourmaline nodules from Capo Bianco aplite (Elba Island, Italy): an example of diffusion limited aggregation growth in a magmatic system. Contributions Mineralogy Petrology 153, 493–508.
Pesquera, A., Velasco, F., 1997. Mineralogy, geochemistry and geological significance of tourmaline-rich rocks from the Paleozoic Cinco Villas massif (western Pyrenees, Spain). Contributions Mineralogy Petrology 129 (1), 53–74.
Plimer, I.R., 1987. The association of tourmalinite with stratiform scheelite deposits. Miner. Deposita 22, 282–291.
Poklepovic, M.F., 2007. Modelado mineralógico, petrológico y geoquímico de sistemas postmagmáticos de interacción fluido-roca en granitoides félsicos de las Sierras Pampeanas Orientales de Córdoba, Santiago del Estero y San Luis, República Argentina. Ph.D. Thesis. Facultad de Ciencias Exactas, Físicas y Naturales, Universidad Nacional de Córdoba, Argentina.
Poklepovic, M.F., Lira, R., 2005. Evidencias del "efecto tetrad" entre las fases fundido-fluido del leucogranito Los Riojanos, Batolito de Achala, Argentina. XVI Congr. Geol. Argent. 1, 639–640.
Potter II, R.W., 1977. Pressure corrections for fluid-inclusion homogenization temperatures based on the volumetric properties of the system NaCl-H_2O. J. Res. U.S. Geol. Surv. 5, 603–607.
Pouchou, J.L., Pichoir, F., 1985. PAP' (phi-rho-z) procedure for improved quantitative microanalysis. In: Armstrong, J.T. (Ed.), Microbeam Analysis. San Francisco Press, San Francisco, pp. 104–106.
Ragland, P.C., 1989. Basic Analytical Petrology. Oxford University Press, New York.
Rapela, C.W., Baldo, E.G., Pankhurst, R.J., Fanning, C.M., 2008. The Devonian Achala Batholith of the Sierras Pampeanas: F-rich, Aluminous A-type Granites. 6_{th}

South American Symposium on Isotope Geology, CD-ROM. San Carlos de Bariloche, Argentina.
Roedder, E., 1984. Fluid Inclusions. Reviews in Mineralogy, vol. 12. Mineralogical Society of America, Virginia.
Rossi, J.N., Toselli, A.J., Saavedra, J., Sial, A.N., Pellitero, E., Ferreira, V.P., 2002. Common crustal source for contrasting peraluminous facies in the early paleozoic Capillitas batholith, NW Argentina. Gondwana Reserach 5 (2), 325–337.
Rozendaal, A., Bruwer, L., 1995. Tourmaline nodules: indicators of hydrothermal alteration and Sn-Zn-(W) mineralization in the Cape Granite Suite, South Africa. J. Afr. Earth Sci. 21, 141–155.
Samson, I.M., Sinclair, W.D., 1992. Magmatic hydrothermal fluids and the origin of quartz-tourmaline orbicules in the Seagull batholith, Yukon-territory. Can. Mineral. 30, 937–954.
Sharp, Z.D., Aturodei, V., Durakiewicks, T., 2001. A rapid method for determination of hydrogen and oxygen isotope ratios from water and hydrous minerals. Chem. Geol. 178, 197–201.
Shepperd, T.J., Rankin, A.H., Alderton, D.H.M., 1985. A Practical Guide to Fluid Inclusion Studies. Blackie & Son. Ltd, Glasgow.
Shewfelt, D.A., 2005. The Nature and Origin of Western Australian Tourmaline Nodules; a Petrologic, Geochemical and Isotopic Study. Master Thesis. University of Saskatchewan, Saskatoon, Canada.
Sillitoe, R.H., 1985. Ore-related breccias in vulcanoplutonic arcs. Econ. Geol. 80, 1467–1515.
Sillitoe, R.H., Sawkins, F.J., 1971. Geologic, mineralogic and fluid inclusion studies relating to the origin of copper-bearing tourmaline breccia pipes, Chile. Econ. Geol. 66, 1028–1041.
Sinclair, W.D., Richardson, J.M., 1992. Quartz-tourmaline orbicules in the Seagull batholith, Yukon territory. Can. Mineral. 30, 923–935.
Skewes, M.A., Holmgren, C., Stern, C.R., 2003. The Donoso copper-rich, tourmaline-bearing breccia pipe in central Chile: petrologic, fluid inclusion and stable isotope evidence for an origin from magmatic fluids. Miner. Deposita 38, 2–21.
Slack, J.F., 1982. Tourmalines from Appalachian-Caledonian massive sulfide deposits and its exploration significance. Trans. Institution Min. Metallurgy 91, B81–B89.
Slack, J.F., 1996. Tourmaline associations with hydrothermal ore deposits. In: Grew, E.S., Anovitz, L.M. (Eds.), Boron: Mineralogy, Petrology and Geochemistry. Reviews in Mineralogy, vol. 33, pp. 559–643.
Slack, J.F., Herriman, N., Barnes, R.G., Plimer, I.R., 1984. Stratiform tourmalinites in metamorphic terrains and their geologic significance. Geology 12, 713–716.
Slack, J.F., Palmer, M.R., Stevens, B.P., Barnes, R.G., 1993. Origin and significance of tourmaline-rich rocks in the Broken Hill district, Australia. Econ. Geol. 88, 505–541.
Strong, D.F., 1994. A model for granophile mineral deposits. In: Roberts, R.G., Shearan, P.A. (Eds.), Ore Models. Geoscience Canada, pp. 59–66.
Takahashi, Y., Yoshida, H., Sato, N., Hama, K., Yusa, Y., Shimizu, H., 2002. W- and M-type tetrad effects in REE patterns for water-rock systems in the Tono uranium deposits, central Japan. Chem. Geol. 184, 311–335.
Taylor, B.E., Slack, J.F., 1984. Tourmalines from Appalachian-Caledonian massive sulfide deposits: textural, chemical, and isotopic relationships. Econ. Geol. 79, 1703–1726.
Tejerina, L.E., 1985. Geología de la manifestación uranífera “El Flaco”, características metalogenéticas. Graduate Thesis. Facultad de Ciencias Exactas, Físicas y Naturales, Universidad Nacional de Córdoba, Argentina.
Trumbull, R.B., Krienitz, M.-S., Gottesman, B., Wiedenbeck, M., 2008. Chemical and boron-isotope variations in tourmalines from an S-type granite and its source rocks: the Erongo granite and tourmalinites in the Damara Belt, Namibia. Contributions Mineralogy Petrology 155, 1–18.
Viramonte, J.M., Becchio, R.A., Viramonte, J.G., Pimentel, M.M., Martino, R.D., 2007. Ordovician igneous and metamorphic units in southeastern Puna: new U–Pb and Sm–Nd data and implications for the evolution of northwestern Argentina. J. S. Am. Earth Sci. 24, 167–183.
Wolf, M.B., London, D., 1997. Boron in granitic magmas: stability of tourmaline in equilibrium with biotite and cordierite. Contributions Mineralogy Petrology 130, 12–30.
Yavuz, F., Gültekin, A.H., Karakaya, M.Ç., 2002. CLASTOUR: a computer program for classification of the minerals of the tourmaline group. Comput. Geosciences 28, 1017–1036.
Zhenhua, Z., Xiaolin, X., Xiaodong, H., Yixian, W., Quiang, W., Zhiwei, B., Jahn, B., 2002. Controls on the REE tetrad effect in granites: evidence from the Qianlishan and Baerzhe granites, China. Geochem. J. 36, 527–543.